Sensitivity of Idealized Squall-Line Simulations to the Level of Complexity Used in Two-Moment Bulk Microphysics Schemes

KWINTEN VAN WEVERBERG AND ANDREW M. VOGELMANN

Brookhaven National Laboratory, Upton, New York

HUGH MORRISON

National Center for Atmospheric Research, Boulder, Colorado*

JASON A. MILBRANDT

Numerical Weather Prediction Research Section, Environment Canada, Dorval, Quebec, Canada

(Manuscript received 9 May 2011, in final form 13 October 2011)

ABSTRACT

This paper investigates the level of complexity that is needed within bulk microphysics schemes to represent the essential features associated with deep convection. To do so, the sensitivity of surface precipitation is evaluated in two-dimensional idealized squall-line simulations with respect to the level of complexity in the bulk microphysics schemes of H. Morrison et al. and of J. A. Milbrandt and M. K. Yau. Factors examined include the number of predicted moments for each of the precipitating hydrometeors, the number and nature of ice categories, and the conversion term formulations. First, it is shown that simulations of surface precipitation and cold pools are not only a two-moment representation of rain, as suggested by previous research, but also by two-moment representations for all precipitating hydrometeors. Cold pools weakened when both rain and graupel number concentrations were predicted, because size sorting led to larger graupel particles that melted into larger raindrops and caused less evaporative cooling. Second, surface precipitation was found to be less sensitive to the nature of the rimed ice species (hail or graupel). Production of hail in experiments including both graupel and hail strongly depends on an unphysical threshold that converts small hail back to graupel, indicating the need for a more physical treatment of the graupel-to-hail conversion. Third, it was shown that the differences in precipitation extremes between the two-moment microphysics schemes are mainly related to the treatment of drop breakup. It was also shown that, although the H. Morrison et al. scheme is dominated by deposition growth and low precipitation efficiency, the J. A. Milbrandt and M. K. Yau scheme is dominated by riming processes and high precipitation efficiency.

1. Introduction

A proper representation of deep convection is of primary importance to climate models and numerical weather prediction (NWP) models, because the latent heat associated with it drives atmospheric circulations. It is also associated with the most intense precipitation events occurring in the midlatitudes and the tropics. Many NWP models now operate at convection permitting horizontal grid spacing of only a few kilometers, at which convection parameterizations are typically not needed. This has brought the role of microphysics in the simulation of deep convection in the middle of the research spotlight over recent years (e.g., McCumber et al. 1991; Gilmore et al. 2004; Dawson et al. 2010; Morrison and Milbrandt 2011, hereafter MM11).

Bulk microphysics schemes are the workhorses in NWP and climate modeling, which typically apply conversion formulations to one or more bulk quantities of the particle size distribution of a number of hydrometeors. A

* The National Center for Atmospheric Research is sponsored by the National Science Foundation.

Corresponding author address: Kwinten Van Weverberg, Brookhaven National Laboratory, Environmental Sciences Brookhaven National Laboratory, Building 490-D, Upton, NY 11973.
E-mail: kvweverberg@bnl.gov

DOI: 10.1175/MWR-D-11-00120.1

variety of such bulk microphysics parameterizations have been developed over the past decades, with gradually increasing complexity. The most basic of these schemes predict only the mixing ratio of a few hydrometeor types (''one-moment schemes''). Typically, such models contain precipitating and nonprecipitating liquid (Kessler 1969) and ice water (Cotton et al. 1982). Later, complexity was added to those models by including different ice categories, such as graupel (Rutledge and Hobbs 1984), hail (Lin et al. 1983), and even up to 10 ice categories (Straka and Mansell 2005). Other models tend to have more complexity by predicting not only the mixing ratio but also the number concentration of the hydrometeors (''two-moment schemes''; e.g., Ferrier 1994; Morrison et al. 2009, hereafter MTT; Seifert and Beheng 2001) and the radar reflectivity (''three-moment schemes''; e.g., Milbrandt and Yau 2005b, hereafter MY). The most complex schemes have left the bulk assumption of the different predicted water species and apply microphysical formulations to several separate size distribution bins (''spectral schemes''; e.g., Kogan 1991; Khain et al. 1999). However, because these spectral models are much more computationally expensive than bulk schemes, they are not yet used operationally. Although bulk microphysics schemes with prognostic hydrometeors were developed mainly for NWP, they are now being more commonly used in climate models (e.g., Morrison and Gettelman 2008; Song and Zhang 2011), particularly as enhanced computational resources enable climate models to operate at horizontal grid spacings comparable to those in NWP.

Given the computational burden these complex bulk parameterizations impose on NWP and climate simulations, a critical question to be answered is what level of complexity is needed to represent the essential features associated with deep convection. A number of publications suggest adding complexity to existing bulk microphysics schemes by increasing the number of ice categories for the simulation of convective and stratiform precipitation (McCumber et al. 1991; Ferrier et al. 1995; Van Weverberg et al. 2011a). They showed that this increased the overall realism of their simulations. Further, two-moment schemes have been shown to capture better than one-moment schemes the structure of supercells (Milbrandt and Yau 2006b; Dawson et al. 2010) and squall lines (MTT), whereas other studies have shown sensitivity but no clear improvement with a higher number of prognostic moments (Milbrandt et al. 2010; Varble et al. 2011). The performances of triple-moment schemes are overall similar to two-moment schemes (Dawson et al. 2010; Milbrandt and Yau 2006; Milbrandt et al. 2010). It remains debatable, however, whether increased computing power should be primarily used to increase the number of hydrometeor classes or the number of predicted moments. Similarly, although most of the previous work investigated fully one-moment and fully two-moment schemes, there is little published work on the impact of separately predicting more moments of each hydrometeor class.

Another outstanding issue regarding complex microphysics parameterizations is the reason for the considerable variation in the behavior of similarly complex models (e.g., MM11). As long as it is unknown why these models differ in terms of surface precipitation and the representation of moist convection, it will remain a challenge to learn from model–observation comparisons and bring forward ways for model improvement.

To address these issues, this paper describes a number of sensitivity experiments imposed on an idealized 2D squall-line simulation within the context of two commonly used two-moment microphysics schemes (MTT; MY). First, we examine the role of the number of predicted moments for each precipitating hydrometeor class separately by changing fully one-moment versions of the aforementioned schemes step by step (hydrometeor class by hydrometeor class) to the fully two-moment schemes. Second, we increased the number of precipitating ice categories by extending versions of both schemes, which contain only snow and graupel as precipitating ice categories, to also include hail. A last set of experiments was designed to understand why similar versions of both schemes still yield considerable differences in terms of surface precipitation and moist processes aloft. To that end, we systematically replaced parts of one microphysics scheme by the formulations of the other scheme until both schemes became identical.

The next section discusses the model setup applied in all these experiments, which are explained in detail in section 2b. Results are documented in section 3, which are discussed and summarized in section 4.

2. Model description and experimental design

a. Model description

The Advanced Research Weather Research and Forecasting model (ARW-WRF) version 3.2 (Skamarock et al. 2007) was used for all experiments, applying the standard 2D idealized squall-line case available within the WRF package. Initialization of the model was done using the environmental sounding of Weisman and Klemp (1984), which represents a midlatitude continental squall-line environment. The 2D framework allows for a large number of experiments, yet still captures the essential structure perpendicular to the line of propagation. The domain consisted of a 600 km $\times$ 20 km vertical cross

TABLE 1. Values of constants and parameters used in the size distribution formulations of MY and MTT throughout all simulations.

Parameter	Value	Reference
V–D coef for rain (a_{vr})	149.1	Tripoli and Cotton (1980)
V–D coef for cloud ice (a_{vi})	71.34	Ferrier (1994)
V–D coef for snow (a_{vs})	11.72	Locatelli and Hobbs (1974)
V–D coef for graupel (a_{vg})	19.3	Ferrier (1994)
V–D coef for hail (a_{vh})	206.89	Ferrier (1994)
V–D exponent for rain (b_{vr})	0.5	Tripoli and Cotton (1980)
V–D exponent for cloud ice (b_{vi})	0.6635	Ferrier (1994)
V–D exponent for snow (b_{vs})	0.41	Locatelli and Hobbs (1974)
V–D exponent for graupel (b_{vg})	0.37	Ferrier (1994)
V–D exponent for hail (b_{vh})	0.6384	Ferrier (1994)
m–D coef for all hydrometeors (a_{mx})	(π/6ρ_x)	
m–D coef for all hydrometeors (b_{mx})	3	

section with a horizontal grid spacing of 1 km and a vertical grid spacing of 250 m. Turbulence was represented by a 1.5-order turbulent kinetic energy (TKE) scheme, whereas radiation and boundary layer processes were turned off. All simulations were integrated over 5 h.

Microphysical processes are represented by either the MTT or the MY two-moment schemes. Both schemes were modified from the original version in WRF version 3.2 in order to provide them with identical size distribution assumptions. Both schemes include two-moment cloud water and ice and have three precipitating hydrometeor classes: rain, snow, and graupel. MY also has a separate category for hail, but it was shut off for several simulations in this study for direct comparison to MTT. Relevant prescribed size distribution and fall speed parameters are listed in Table 1, which were set to be identical for both schemes. In this study, the size distributions of all precipitating hydrometeors in both schemes are represented by inverse exponential functions of the form

$$N_x(D) = N_{0x} e^{-\lambda_x D}, \tag{1}$$

where N_{0x} and λ_x are the intercept and slope parameters, respectively, and D is the particle diameter. The slope parameter can be calculated from the mixing ratio q_x (in kg kg^{-1}) and number concentration N_x (in kg^{-1}) by

$$\lambda_x = \left[\frac{a_{mx} N_x \Gamma(b_{mx} + 1)}{q_x}\right]^{1/(b_{mx})}, \tag{2}$$

where a_{mx} and b_{mx} are the parameters of the mass–diameter power-law relation, listed in Table 1. In contrast

TABLE 2. Intercept parameter N_{0x} used in the one-moment experiments and density ρ_x for all precipitating hydrometeor categories.

Category	N_{0x} (m^{-4})	ρ_x (kg m^{-3})
Rain	1×10^7 (Dudhia 1989)	1000
Snow	2×10^7 (Dudhia 1989)	100
Graupel	4×10^6 (Rutledge and Hobbs 1984)	400
Hail	1×10^5 (Milbrandt and Yau 2005b)	900

to the original formulations of MY, all hydrometeors in the simulations presented here are assumed to be spherical. Mass and number-concentration-weighted bulk fall velocities for all hydrometeor species are calculated based on empirical power-law velocity–diameter relationships,

$$V_x(D) = a_{vx} D^{b_{vx}}, \tag{3}$$

where a_{vx} and b_{vx} are empirically derived parameters, listed in Table 1.

To make a close comparison between both schemes, continental aerosol concentrations were prescribed in both schemes, where these concentrations followed a lognormal distribution in the MTT and a polynomial distribution in MY. This leads to lower aerosol concentrations in MY, mainly at lower altitudes. Ice nucleation followed Cooper (1986).

b. Experiment design

1) NUMBER OF PREDICTED MOMENTS

A first set of experiments is designed to understand whether a two-moment approach is necessary for all precipitating hydrometeors or whether a one-moment approach is sufficient to simulate the essential features associated with deep convection. A first experiment implemented the fully two-moment versions of the MTT and the MY schemes (MTT-BASE and MY-BASE). Subsequent experiments consisted of modifying, one by one, the representation of precipitating hydrometeors to only predict one moment of their respective distributions. First, graupel number concentration was diagnosed instead of predicted, whereas rain and snow number concentrations were still explicitly predicted (MTT-2R2S1G and MY-2R2S1G). Second, both snow and graupel number concentrations were diagnosed, yet rain number concentration was still predicted (MTT-2R1S1G and MY-2R1S1G). Finally, both schemes were made fully one moment for each of the hydrometeors (MTT-1R1S1G and MY-1R1S1G), except for cloud ice and cloud water, which remained two moment in all experiments. The implementation of a one-moment approach for each specie requires the specification of the intercept N_{0x} of the size distribution [Eq. (1)]. Table 2 lists the values for N_{0x}, as

TABLE 3. Experiment overview. Boldface font indicates baseline simulations.

Experiment name	Description
MTT-BASE	**Baseline two-moment simulation (**MTT**)**
MTT-2R2S1G	Same as MTT-BASE, except for one-moment graupel
MTT-2R1S1G	Same as MTT-BASE, except for one-moment graupel and snow
MTT-1R1S1G	Same as MTT-BASE, except for one-moment graupel, snow, and rain
MTT-H	Same as MTT-BASE, except for rimed ice category set to hail
MTT-GH	Same as MTT-BASE, except for additional ice category for hail
MTT-GH-NT	Same as MTT-GH, except for removed the hail-to-graupel threshold
MTT-WM	Same as MTT-BASE, except for the warm rain and melting formulations and size limiters for all species set to those of MY
MTT-WM-BRK	Same as MTT-WM, except for breakup formulations set back to those of MTT-BASE (breakup threshold 300 μm)
MTT-WM-ICE	Same as MTT-WM, except for ice, snow, and graupel deposition and autoconversion set to those of MY
MTT-WM-ICE-GDP	Same as MTT-WM-ICE, except for graupel sublimation formulations set back to those of MTT-BASE (active sublimation)
MTT-WM-ICE-COL	Same as MTT-WM-ICE, except for collection formulations set to those of MY
MY-BASE	**Baseline two-moment simulation (**MY**)**
MY-2R2S1G	Same as MY-BASE, except for one-moment graupel
MY-2R1S1G	Same as MY-BASE, except for one-moment graupel and snow
MY-1R1S1G	Same as MY-BASE, except for one-moment graupel, snow, and rain
MY-H	Same as MY-BASE, except for rimed ice category set to hail
MY-GH	Same as MY-BASE, except for additional ice category for hail
MY-GH-NT	Same as MY-GH, except for removed hail-to-graupel threshold

well as the density applied for each specie. The number concentration N_x in the one-moment approach was diagnosed following

$$N_X = \frac{N_{0X}}{\lambda_X}. \quad (4)$$

2) NUMBER AND NATURE OF PREDICTED ICE CATEGORIES

A second set of experiments investigates the impact of increasing the number of precipitating ice categories to three. To do so, we extended the fully two-moment versions of both microphysics schemes as described

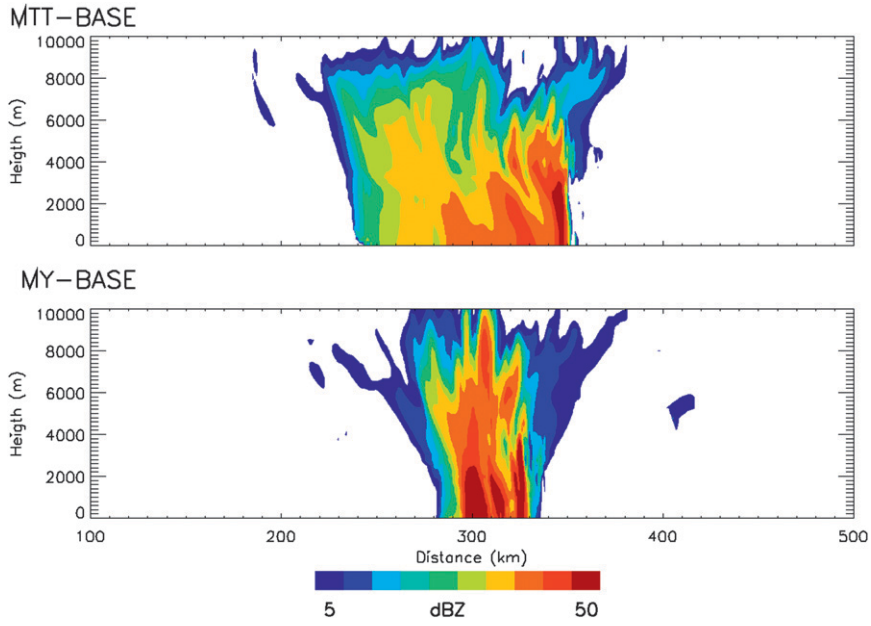

FIG. 1. Vertical cross sections of radar reflectivity for (top) the MTT-BASE and (bottom) the MY-BASE at 4 h and 30 min into the simulation.

TABLE 4. Surface-precipitation characteristics in all MTT experiments after 5 h of simulation. Column headers are, from left to right, domain-average 5-h accumulated surface precipitation, domain-maximum 5-h accumulated surface precipitation, PE, domain- and time-integrated updraft latent heat released (LH; vertical velocity >1 m s^{-1}), and domain- and time-integrated low-level updraft kinetic energy (LLKE; vertical velocity >1 m s^{-1} between the surface and 3000-m altitude). LH includes heat released by all microphysical processes within the updraft (condensation, evaporation, freezing, melting, deposition, and sublimation). Values in parentheses denote the difference relative to the baseline simulations, where smaller (larger) than 1 indicates lower (higher) values than baseline. Boldface font indicates the baseline simulation.

	Mean (mm)	Max (mm)	PE (%)	LH (10^{16} J s)	LLKE (10^{16} J s)
MTT-1R1S1G	4.4 (1.01)	84.3 (0.83)	29.4 (0.85)	4.091 (1.17)	0.937 (1.14)
MTT-2R1S1G	4.5 (1.03)	88.7 (0.87)	28.2 (0.82)	4.381 (1.25)	1.029 (1.26)
MTT-2R2S1G	4.9 (1.12)	98.1 (0.97)	33.7 (0.98)	3.892 (1.11)	0.927 (1.13)
MTT-BASE	**4.3**	**101.4**	**34.5**	**3.496**	**0.819**
MTT-H	5.0 (1.16)	142.1 (1.40)	38.3 (1.11)	3.597 (1.03)	0.855 (1.04)
MTT-GH	4.0 (0.93)	79.7 (0.79)	24.2 (0.70)	4.750 (1.36)	1.052 (1.28)
MTT-GH-NT	4.9 (1.12)	121.1 (1.19)	36.3 (1.05)	3.649 (1.04)	0.911 (1.11)
MTT-WM-BRK	5.0 (1.15)	111.2 (1.10)	36.4 (1.06)	3.641 (1.04)	0.785 (0.96)
MTT-WM	4.6 (1.06)	181.3 (1.79)	39.0 (1.13)	3.287 (0.94)	0.754 (0.92)
MTT-WM-ICE-GDP	5.1 (1.18)	175.6 (1.73)	39.3 (1.14)	3.682 (1.05)	0.752 (0.92)
MTT-WM-ICE	5.6 (1.28)	204.4 (2.02)	47.0 (1.37)	3.399 (0.97)	0.780 (0.95)
MTT-WM-ICE-COL	5.3 (1.22)	187.5 (1.85)	50.5 (1.47)	3.078 (0.88)	0.711 (0.87)

above (MTT-BASE and MY-BASE) to also include hail along with graupel (MTT-GH and MY-GH). The implementation of an additional ice category requires several additional conversion terms. In the original formulations of MY, graupel and hail were present; we applied the MY scheme accordingly for the MY-GH experiment. For the MTT-GH experiment, the collection by hail of cloud water, rain, and snow was implemented according to the collection formulations of these categories by graupel in the MTT-BASE scheme. Further, freezing of raindrops was added as a source term for hail (not graupel), and the conversion of graupel to hail was implemented as described in MY. For the three-category interactions that can result in graupel or hail (i.e., collection of rain by graupel and cloud ice by rain), parameterization is done based on the resulting bulk density of the destination particle, consistent with MY. Further, we implemented a size threshold of 5.0 mm, below which hail would be converted back to graupel in the MTT-GH experiment, consistent with the original formulation of the MY-GH scheme.

An additional experiment was performed with only two precipitating ice categories but including hail along with snow instead of graupel (MTT-H and MY-H). Source and loss terms for hail in these simulations were the same as those for graupel in the MTT-BASE and MY-BASE experiments, so that the only difference between the hail-only and the graupel-only experiments consisted of modified constants for the *m–D* and *V–D* relationships, which are provided in Table 1.

3) CONVERSION PROCESS FORMULATIONS

A last set of experiments was designed to examine the role of the conversion term formulations in order to understand why the MTT-BASE and MY-BASE schemes yield considerable differences in their representation of moist processes and surface precipitation despite their similar level of complexity (MM11). The microphysical conversion processes were divided into three groups, being ''warm rain processes,'' ''ice deposition and initiation processes,'' and ''collection processes.'' Each of these three groups of processes was investigated by making the conversion terms that comprise them equal in both schemes. The MTT-BASE scheme was arbitrarily chosen as the scheme that was gradually modified by implementing the formulations of the MY-BASE scheme, until both schemes were identical in terms of parameterized processes. An overview of all processes active in the baseline simulations is provided in appendix A.

First, the warm rain scheme based on Cohard and Pinty (2000), as used in MY, was implemented in the MTT-BASE scheme (MTT-WM). A second experiment also implemented all processes associated with precipitating and nonprecipitating ice initiation, deposition, and ice-to-snow autoconversion of the MY scheme into the MTT-WM scheme (MTT-WM-ICE). Last, the MTT-WM-ICE scheme was further modified with the collection terms and efficiencies from the MY scheme (MTT-WM-ICE-COL) and hence was basically identical to the MY-BASE scheme. A detailed description of which processes were changed in each of these experiments is provided in appendix B. An overview of all experiments and their specifications is provided in Table 3.

3. Results

a. Number of predicted moments

Figure 1 shows vertical cross sections of the radar reflectivity for both the MTT-BASE and the MY-BASE

TABLE 5. As in Table 4, but for the MY experiments.

	Mean (mm)	Max (mm)	PE (%)	LH (10^{16} J s)	LLKE (10^{16} J s)
MY-1R1S1G	5.8 (1.11)	144.5 (0.74)	43.8 (0.88)	3.659 (1.21)	0.890 (1.24)
MY-2R1S1G	5.9 (1.12)	170.1 (0.87)	45.0 (0.91)	3.610 (1.19)	0.858 (1.19)
MY-2R2S1G	6.0 (1.14)	181.3 (0.93)	44.2 (0.89)	3.804 (1.26)	0.870 (1.21)
MY-BASE	**5.3**	**195.6**	**49.5**	**3.029**	**0.720**
MY-H	5.7 (1.08)	179.5 (0.92)	42.5 (0.86)	3.700 (1.22)	0.829 (1.15)
MY-GH	5.2 (0.98)	153.8 (0.79)	40.3 (0.81)	3.508 (1.16)	0.938 (1.30)
MY-GH-NT	6.2 (1.18)	214.8 (1.10)	49.2 (0.99)	3.573 (1.18)	0.846 (1.18)

simulations, showing a well-formed squall line in both simulations. However, the trailing stratiform area in the MTT-BASE experiment is more developed compared to MY-BASE. The 5-h accumulated surface-precipitation characteristics for all experiments can be found in Tables 4 and 5 and are depicted in Fig. 2. None of the experiments on the number of predicted moments led to surface-precipitation changes beyond 15% as compared to the baseline simulations (MTT-BASE and MY-BASE), which is consistent with MTT.

Microphysics can affect surface precipitation generally in two possible ways. First, microphysics schemes have different ways of handling the transition from the available water vapor supersaturation over the different slow (e.g., cloud water) or fast-falling (e.g., hail) hydrometeors to fallout as rain to the surface. Some microphysics schemes tend to favor formation of slow precipitation or have more intense re-evaporation of condensate; others favor a fast fallout of precipitation. A measure to quantify this effect is the precipitation efficiency (PE), defined here following Sui et al. (2007),

$$\mathrm{PE} = \frac{P}{\mathrm{vaporloss}}, \tag{5}$$

where P is the domain-total surface precipitation (kg) and "vapor loss" is all vapor consumed by the microphysics parameterization across the same domain (kg). Vapor can be consumed by cloud water condensation, graupel, snow and ice deposition, or ice initiation. A second way that microphysics schemes can affect the surface precipitation is by interacting with the dynamics, by the release of large amounts of latent heat associated with condensation or freezing processes or by affecting cold-pool development. To determine whether differences in surface precipitation between the different experiments are predominantly due to the former or the latter effect, Tables 4 and 5 provide the PE (more directly related to microphysics) and the domain-average

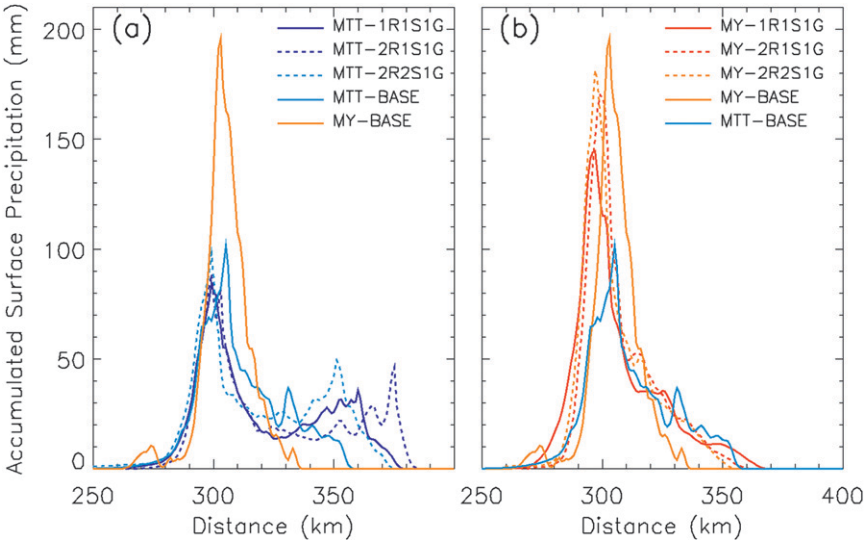

FIG. 2. Spatial distribution of accumulated surface precipitation over the full time integration of 5 h for the experiments on the number of predicted moments for (a) the MTT scheme (blue) and (b) the MY scheme (red). The baseline simulations of the MY and MTT schemes have been added for reference.

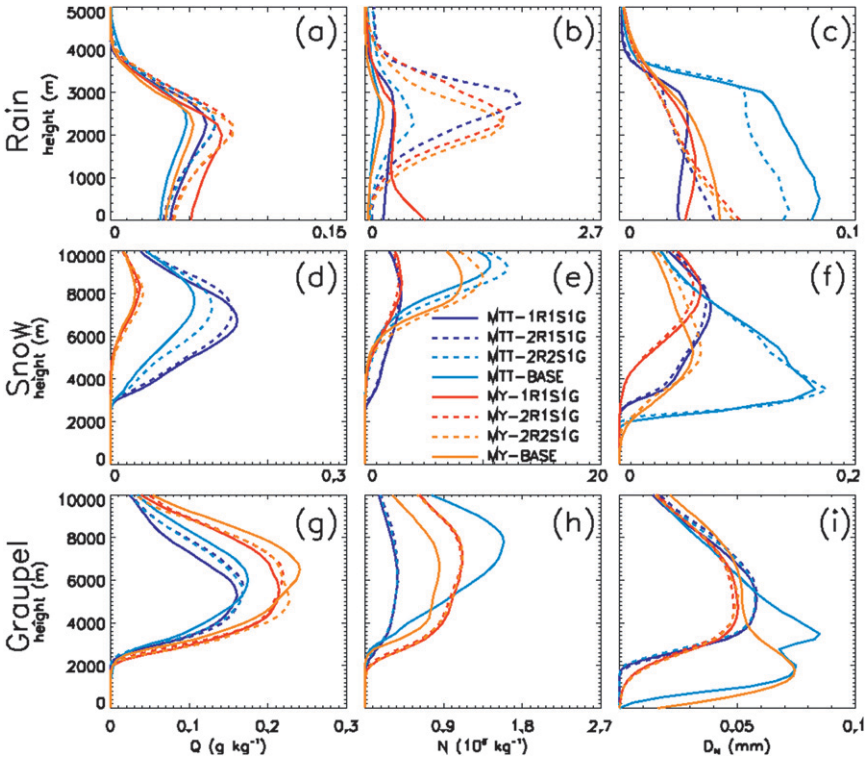

FIG. 3. Domain- and time-averaged vertical profiles of (left) mixing ratio, (middle) number concentration, and (right) number-weighted mean particle diameter for (top) rain, (middle) snow, and (bottom) graupel and for all experiments on the number of predicted moments. MTT experiments are represented in blue and MY experiments in red. Note the different scales of the *x* axes for the different hydrometeors and the different scale of the *y* axis for the rain species.

updraft latent heat release for each experiment (more related to microphysics–dynamics interaction).

Implementing a two-moment formulation for rain (MTT-2R1S1G and MY-2R1S1G), as opposed to a one-moment formulation (MTT-1R1S1G and MY-1R1S1G), does not significantly affect surface precipitation, PE, or latent heat (Tables 4, 5). Apart from rain in the MY scheme, the vertical hydrometeor mixing ratios are also little changed (Figs. 3a,d,g). A more pronounced change occurs in the rain number concentrations, mainly just below the melting level. More numerous (and smaller) raindrops are present near this level in the 2R1S1G experiments compared to the 1R1S1G experiments (Fig. 3b). Further, a slight increase in the domain-maximum precipitation occurs in the MTT-2R1S1G, whereas a more pronounced increase occurs in the MY-2R1S1G experiment. Figure 4 provides time-averaged vertical profiles of rain mixing ratio, drop size, and evaporation associated with the location of the largest surface-precipitation accumulation. Although this profile does not provide the exact vertical pathway associated with the most intense surface precipitation (because of vertical and horizontal advection within the storm), this figure can serve as a good approximation for this pathway. Obviously, predicting the number concentration of rain explicitly allows size sorting of drops to take place (e.g., Milbrandt and Yau 2005a). On average across the domain, this leads to smaller drops aloft and larger drops near the surface (Fig. 3c), which has little effect on total rain evaporation. However, in the region with heavy precipitation, raindrops grow larger and hence fall faster as they approach the surface (Figs. 4c,d). Note that, despite the larger near-surface drop size in the MTT-2R1S1G compared to the MTT-1R1S1G, rain evaporation is not decreased at all (and is even slightly higher; Fig. 4e). Indeed, besides raindrop size, rain evaporation is also a function of atmospheric humidity. In the MTT-1R1S1G, the boundary layer moistens very rapidly over time, because evaporation initially is stronger compared to MTT-2R1S1G and the cold pool rapidly becomes colder (not shown). Hence, later in the simulation, further rain evaporation is hindered in the MTT-1R1S1G experiment, whereas it goes on in MTT-2R1S1G. Consequently, there is little difference in rain evaporation between the two experiments over the full time integration. The reason for differences in the impact on drop size between the MY

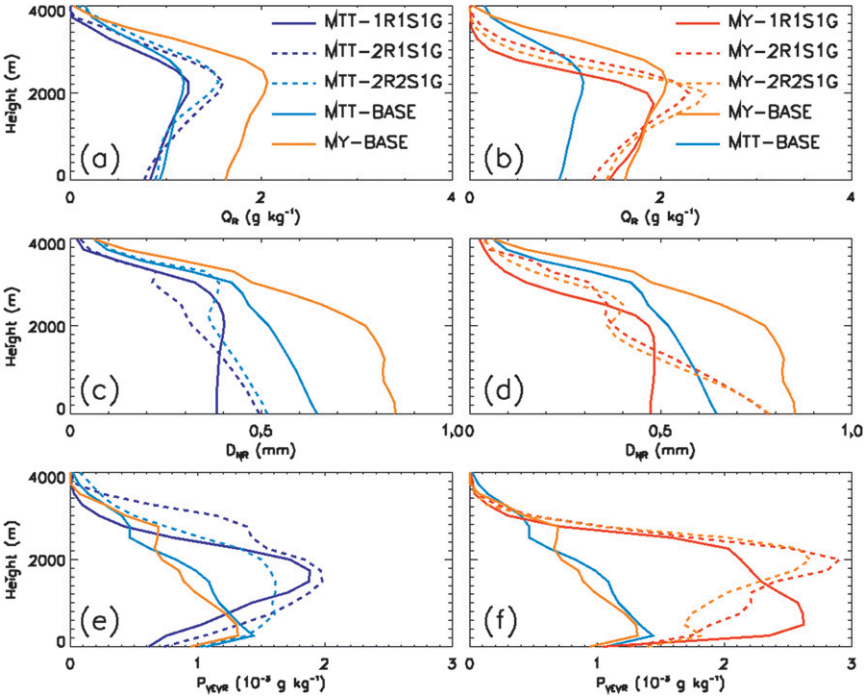

FIG. 4. Time-average vertical profiles (top) of mixing ratio Q_R, (middle) number-weighted mean drop diameter D_{NR}, and (bottom) rain evaporation Pvevr, which all are associated with the location of maximum surface-precipitation accumulation over the full simulation. MTT (left) experiments are represented in blue and MY (right) experiments in red. The baseline simulations of the MY and MTT schemes have been added for reference.

and MTT schemes might be related to the more-active drop breakup parameterization in the latter scheme, as shown in MM11.

In the MTT experiments, an increase in PE occurs when going from one-moment snow (MTT-2R1S1G) to two-moment snow (MTT-2R2S1G). This is accompanied by significant changes in the snow sizes (Fig. 3f). Two-moment snow better represents the effects of the size sorting of snowflakes and the aggregation effect. Therefore, fallout of snowflakes in the midtroposphere is enhanced and the mixing ratio is decreased (Fig. 3d). Note that, in contrast to the fixed N_{0S} in our simulations, one-moment schemes do exist that implement a temperature-dependent N_{0S}. These schemes also tend to better reproduce the larger snow sizes near the freezing level (e.g., Thompson et al. 2004). Figure 5 helps interpret the changes in PE among the different experiments. For a unit amount of vapor consumption (condensation, deposition, and initiation) across the domain and for the full time integration, this figure shows the amount of condensate that is returned to the vapor phase, instead of raining out to the surface. (Note from this figure that sublimation of graupel—and its associated latent cooling—is present in the MTT simulations but is not parameterized in the MY simulations.) The clearest change that occurs between MTT-2R1S1G and MTT-2R2S1G is that the snow sublimation (Pvsbs) is significantly decreased (Fig. 5). This occurs as the residence time of snowflakes aloft is decreased because of their faster fall speeds and because their total effective surface area is reduced (and hence the distribution-integrated capacitance factor) due to their larger size and lower number concentration (Figs. 3e,f). This reduction in sublimation of snow back to vapor increases the PE (Table 4). However, less latent heat is released in the updrafts as well, which offsets the higher PE (Table 4). This reduction could be associated with decreased depositional growth or with the reduced available kinetic energy (Table 4). Because snow is far less abundant in the MY scheme (Fig. 3d), size sorting and aggregation of snow hardly affects the simulation and hence there is little difference between MY-2R1S1G and MY2R2S1G. Domain-maximum precipitation accumulations increased slightly in MY-2R2S1G and MTT-2R2S1G experiments, because of increased rain mixing ratios (Fig. 4a).

A drop of 15%–20% in latent heat release and hence updraft kinetic energy occurs in the MTT-BASE and the MY-BASE experiments compared to the MTT-2R2S1G and MY-2R2S1G experiments, leading to a reduction in domain-average precipitation (Tables 4, 5). Figure 2

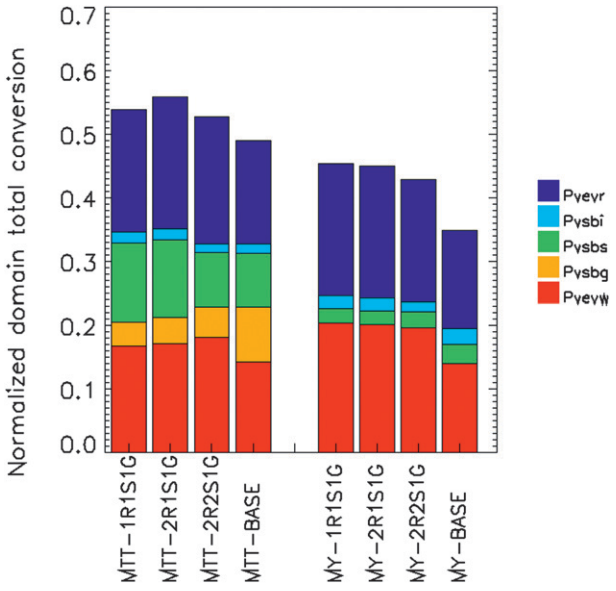

FIG. 5. Domain- and time-integrated total condensate returned to the vapor phase by microphysical processes (given in legend) for each experiment on the number of predicted moments. Values are normalized over the total condensation and deposition for each experiment. Larger normalized total condensate returned to vapor points to lower PE (see appendix B for explanation of the conversion term acronyms).

reveals that this reduction in precipitation occurs mainly in the frontal region of the squall line, whereas the more heavy precipitation in the convective cores is enhanced. To explain this behavior, it is instructive to look at the cold-pool dynamics. Cold pools originate mainly from evaporation of rain and impact the dynamics of storms (Rotunno et al. 1988; Weisman and Rotunno 2004). Figure 6 shows the time evolution of the cold pools for the experiments on the number of predicted moments. In the MTT scheme, it is not until graupel number concentration becomes prognostic that the mean and maximum cold-pool intensity decreases (Figs. 6a,c). In the MY scheme, however, both prognostic rain and graupel number concentrations weaken the cold pools (Figs. 6b,d). It is also clear that the differences in cold-pool intensity between the MTT-2R2S1G and MY-2R2S1G and their respective baseline experiments are larger early in the simulation and become smaller after a few hours. The difference in cold-pool size, however, becomes larger later in the simulations (Figs. 6e,f). In the experiments with rapid onset of cold-pool development and colder cold pools, the air gradually became saturated after some hours, which slows further rain evaporation (not shown). In the experiments with slower onset of cold pools and weaker cold pools, boundary layers remained drier and rain evaporation continued throughout the simulation (not shown). Hence, after some hours the cold-pool temperatures gradually converged in all experiments.

From Fig. 7, the differences in cold-pool strengths between the BASE experiments and their respective 2R2S1G experiments are mainly associated with differences in rain evaporative cooling. The reduction in rain evaporation in the BASE experiments can be related to changes in the rain-size distributions (Fig. 3c). This figure shows that, in the MTT-BASE and the MY-BASE schemes, intense graupel size sorting takes place that leads to larger graupel particles below the freezing level (Fig. 3i). Because melting graupel is the main source for rain, the larger graupel particles also melt into larger raindrops (Fig. 3c), which effectively reduces the rain evaporation and cold-pool intensity (Fig. 6). Previous research has indicated the importance of two prognostic moments for rain on cold-pool development (Milbrandt and Yau 2006; MTT; Dawson et al. 2010; Bryan and Morrison 2012), but our simulations suggest that prognostic graupel number concentration also indirectly affects the cold-pool intensity. The impact of graupel size sorting on the rain-size distribution is also clear from Fig. 8, which shows vertical cross sections of rain and graupel particle sizes through the squall line. This figure also gives a hint as to why surface precipitation in the frontal area of the squall line was reduced within the MTT-BASE and MY-BASE experiments compared to the experiments with one-moment graupel (MTT-2R2S1G and MY-2R2S1G). The larger evaporation of the smaller raindrops in the experiments with one-moment graupel causes stronger cold outflows behind the gust front of the squall line. In the MTT-2R2S1G experiment, discrete propagation, as described by, for instance, Fovell et al. (2006), triggers new cells in front of the squall line (Figs. 8a,e). In the MTT-BASE experiment, the outflow seems to be too weak to do so, and hence less precipitation accumulates in front of the squall line (Figs. 8b,f). No clear cell regeneration in front of the squall line occurs in the MY-2R2S1G experiment, but, even in this case, stronger outflow in the MY-2R2S1G experiments enhances squall-line propagation compared to the MY-BASE experiment, leading to a broader precipitation swath (Figs. 8c,g). From Figs. 6e,f, this also leads to a smaller cold-pool area in the baseline experiments as compared to the experiments with one-moment graupel (MTT-2R2S1G and MY-2R2S1G). This is consistent with the Van Weverberg et al. (2011b) simulations of supercell storms, where the cold-pool areas were more confined when a less evaporation-friendly rain-size distribution was applied. However, because generally less rain evaporates as well (Fig. 5), PE and maximum-precipitation accumulation increase in our simulations. The weaker outflows in the MTT-BASE and MY-BASE experiments and subsequent weaker propagation of the

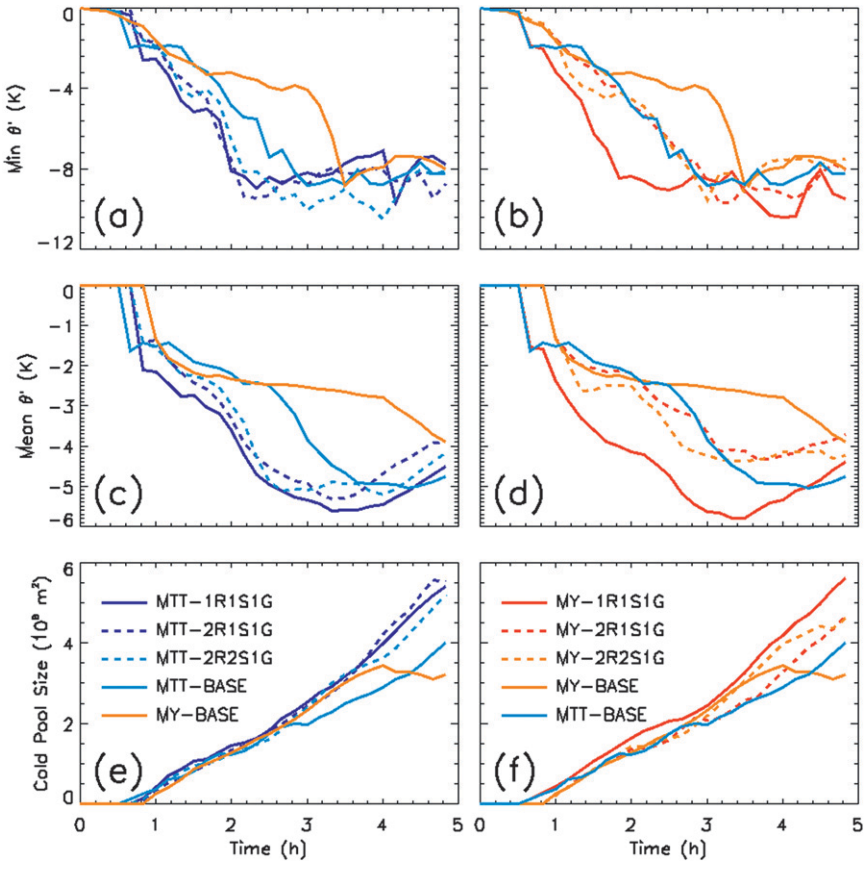

FIG. 6. Time evolution of cold-pool characteristics for all experiments on the number of predicted moments for (left) the MTT scheme and (right) the MY scheme: (top) maximum cold-pool intensity, (middle) mean cold-pool intensity, and (bottom) cold-pool area. Cold pools are defined by the −1-K isotherm of surface potential temperature perturbation. The baseline simulations of the MY and MTT schemes have been added for reference.

squall line might also reduce the entrainment of dry environmental air into the squall lines compared to MTT-2R2S1G and MY-2R2S1G, consistent with somewhat weaker rear-inflow jets in Fig. 8. This might explain the reduced fraction of condensate that is returned to water vapor by cloud water evaporation (Figs. 5, 7) but should be further investigated to yield sound conclusions.

More experiments have been performed with different combinations of one-moment versus two-moment precipitating hydrometeors (1R1S2G and 2R1S2G). A short overview of the results of these experiments is provided in appendix C, which confirm our finding that it is not until two-moment rain is combined with two-moment graupel that the spatial rain distribution narrows and the cold pools weaken. Further, the results in the appendix suggest that excessive number concentrations might arise from certain combinations of one-moment and two-moment hydrometeors, further substantiating the requirement for all precipitation species to follow a two-moment representation.

b. Nature and number of predicted ice categories

A number of previous studies stated that surface precipitation is sensitive to the nature of the rimed precipitating ice species (either graupel or hail) within bulk microphysics schemes (Gilmore et al. 2004; van den Heever and Cotton 2004; MM11; Bryan and Morrison 2012). If the rimed precipitating species were large hail, surface precipitation could increase by as much as 30% (van den Heever and Cotton 2004) and up to 300% (Gilmore et al. 2004) as compared to identical simulations where the largest precipitating ice specie was small graupel. However, most of these studies were performed for 3D supercell simulations and hence were based on rather short simulations (about 2 h). A number of studies showed little sensitivity for real-case simulations and suggested that the strong sensitivity found in real-case simulations might only be valid for certain environmental conditions (Reinhardt and Seifert 2006; Van Weverberg et al. 2011c, manuscript submitted to *Quart.*

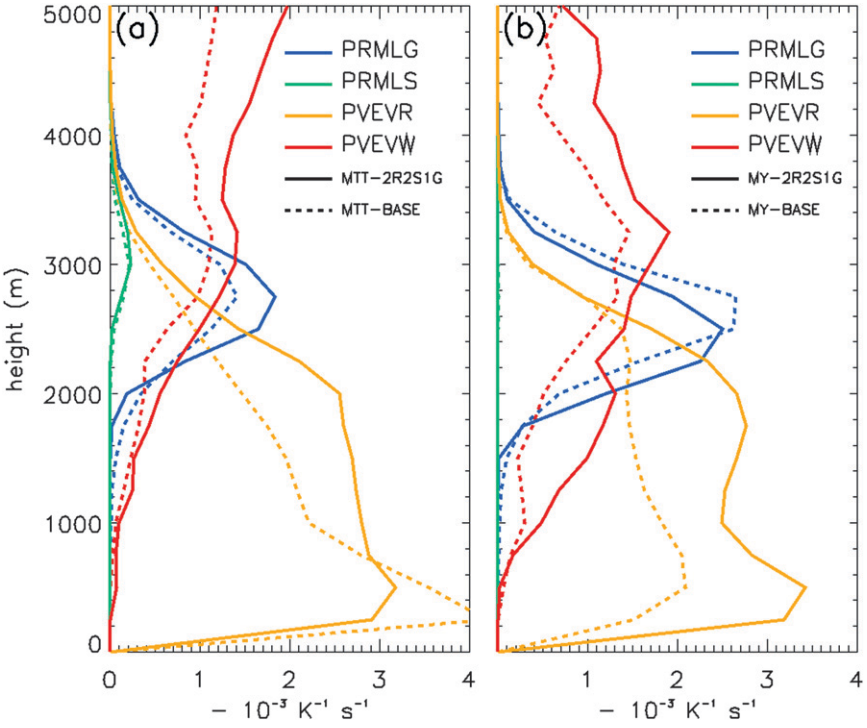

FIG. 7. Vertical profiles of time-averaged cooling rates within downdrafts (vertical velocity < -1 m s^{-1}) associated with several microphysical processes for (a) the MTT scheme and (b) the MY scheme. Solid lines denote the 2R2S1G experiment, and dashed lines denote the BASE experiments.

J. Roy. Meteor. Soc.). Therefore, we investigated whether these conclusions still hold for squall lines and when simulations are integrated over longer periods.

From Tables 4 and 5 and Fig. 9, the inclusion of hail (MTT-H and MY-H) as opposed to graupel (MTT-BASE and MY-BASE) leads the domain-average accumulated precipitation to be only slightly higher after 5 h of simulation. In the MTT-H experiment, the 15% increase in precipitation is due to both a slightly higher PE and enhanced latent heat release as compared to the MTT-BASE experiment. In the MY-H experiment, however, the slight precipitation enhancement (7%) is only due to higher updraft latent heat release. PE is reduced significantly compared to the MY-BASE experiment. The reason for this can be found in the differences in the domain-average vertical profiles of hydrometeor mixing ratio (Fig. 10). It is clear that, although a slight increase in snow mixing ratio occurs in the MTT-H experiment, the MY-H experiment produces as much as 5 times the amount of snow compared to the MY-BASE experiment (Fig. 10d). Figure 11 provides the amount of vapor returned by the microphysics, normalized over the total condensation and deposition for each experiment, which is helpful to interpret the changes in PE. The large growth in snow amounts in the MY-H experiment leads to a large increase in snow sublimation outside the updraft cores. This increased return of vapor from the condensate effectively reduces PE compared to MY-BASE. Enhanced latent heat release can again be associated with differences in cold-pool strength. Figure 12 reveals that cold pools are considerably more intense (Figs. 12a–d) and larger (Figs. 12e,f) in the experiments with large hail as opposed to graupel, because melting hail contributes to the latent cooling down to the surface whereas graupel quickly melts below the melting level. Deeper and larger cold pools again seem to be associated with larger storm systems and more latent heat release; although it might also be that stronger outflow convergence provides additional dynamical forcing (Tables 4, 5). Domain-maximum precipitation is about 40% larger after 5 h of simulation in the MTT-H experiment compared to MTT-BASE, whereas a decrease occurs in the MY-H experiment (Tables 4, 5 and Fig. 9) compared to MY-BASE. It should be mentioned that differences in surface precipitation between the baseline simulations and the simulations including hail were larger earlier into the simulations. Domain-average precipitation (domain-maximum precipitation) was typically 40%–60% (100%–200%) larger in the simulations with hail compared to the baseline simulations 2 h into the simulations (not shown).

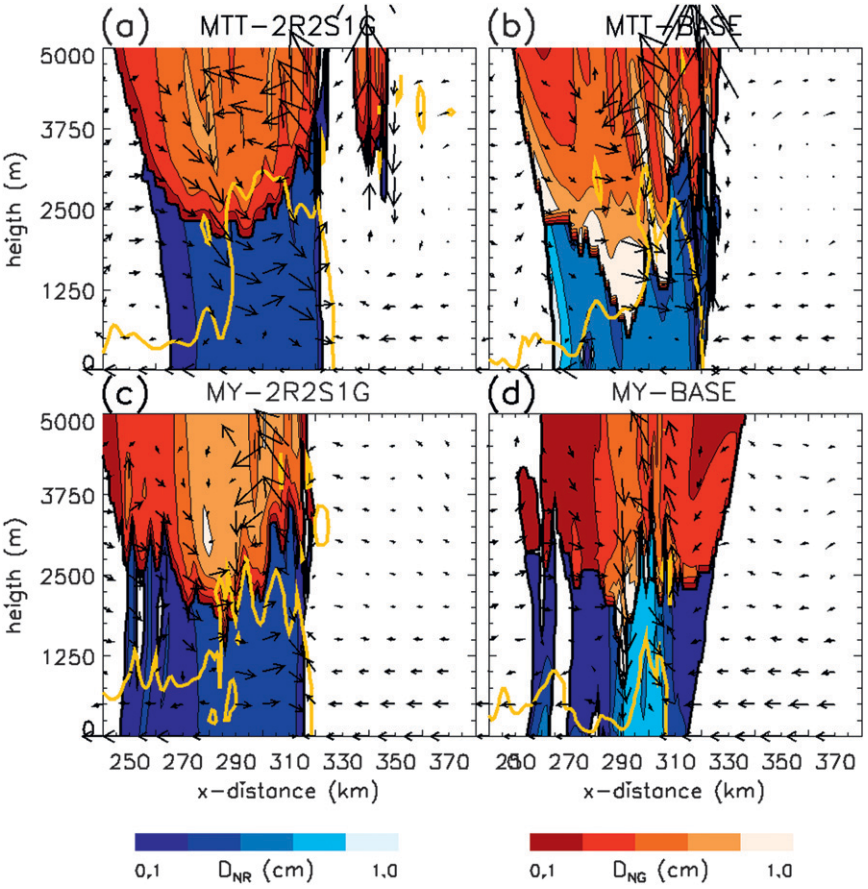

FIG. 8. Vertical cross section through the squall line, (a)–(d) 3 h and 20 min into the simulation and (e)–(h) 3 h and 50 min into the simulation for (a),(e) MTT-2R2S1G; (b),(f) MTT-BASE; (c),(g) MY-2R2S1G; and (d),(h) MY-BASE. Shading indicates number-weighted mean particle size for graupel (red) and rain (blue). Arrows indicate the flow within the squall line, which generally propagates to the right. The yellow solid line indicates the cold-pool boundary (−3-K isotherm).

Further, we investigated the influence of adding ice categories to the simulations by extending the MTT and MY schemes to include both graupel and hail. This was suggested by, for example, McCumber et al. (1991) and Cohen and McCaul (2006) in order to make simulations of convective storms more realistic. The inclusion of both hail and graupel (MTT-GH and MY-GH) has a minor impact on surface precipitation compared to simulations that only contain graupel (MTT-BASE and MY-BASE). A slight decrease in surface precipitation in both schemes is associated with a decrease in PE and an increase in latent heat. From the vertical profiles of the hydrometeors in Fig. 10, the main impact of including both graupel and hail is an increase in the graupel number concentration (Fig. 10h). In the MTT-GH experiment, this effectively increases riming growth of graupel at the expense of snow riming growth (not shown), leading to an increase in graupel mixing ratios and a decrease in snow mixing ratios. Also, graupel depositional growth is enhanced because of the larger number concentration in the MTT-GH experiment, significantly increasing the latent heat release by over 30% (Table 4). However, the more numerous graupel particles are also more prone to sublimation (mainly outside the convective cores), and hence more condensate is returned to the vapor phase. In combination with the much slower fallout by the smaller particles, this dramatically reduces the PE. Because the more numerous graupel particles also affect the rain-size distribution upon melting, PE is further reduced because of enhanced rain evaporation (Fig. 11). In the MY-GH experiment, graupel deposition–sublimation and the associated latent heat release are not parameterized; hence, the dramatic impact of the more numerous particles on deposition and sublimation does not occur. The higher number concentration of graupel still leads to smaller raindrops and more evaporation however, and

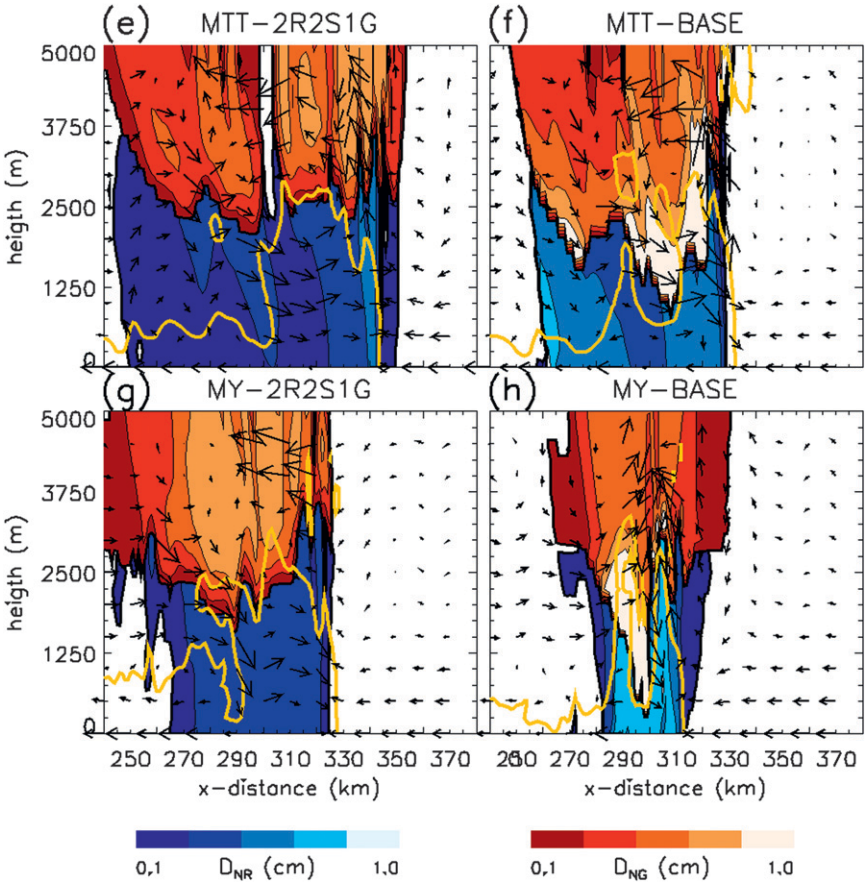

FIG. 8. (*Continued*)

hence PE is reduced also in this experiment as compared to MY-BASE (Table 5 and Fig. 11). As in the MTT-GH experiment, this is counterbalanced by a larger latent heat release (Table 5), which might be associated with larger, deeper cold pools connected to the enhanced rain evaporation in this case (Fig. 12d). The larger evaporation of rain and the smaller, slower-falling raindrops also cause the domain-maximum precipitation accumulation

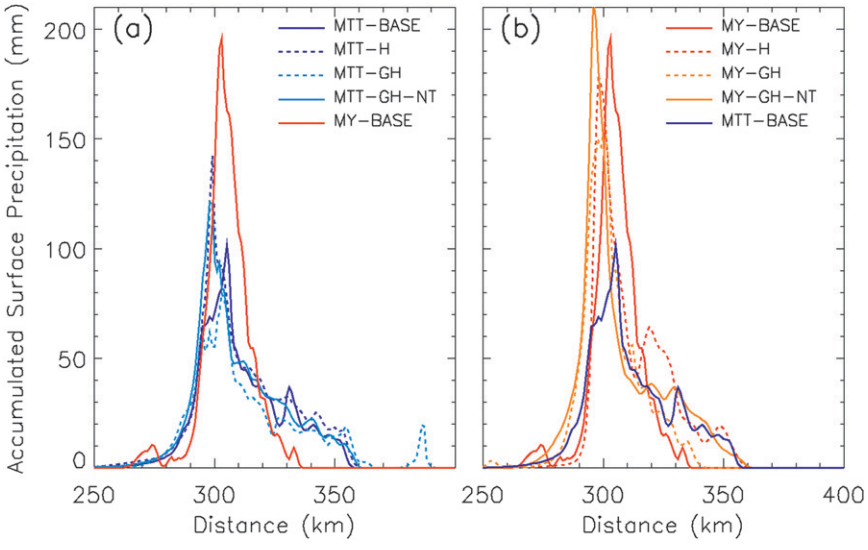

FIG. 9. As in Fig. 2, but for experiments on the number of ice categories.

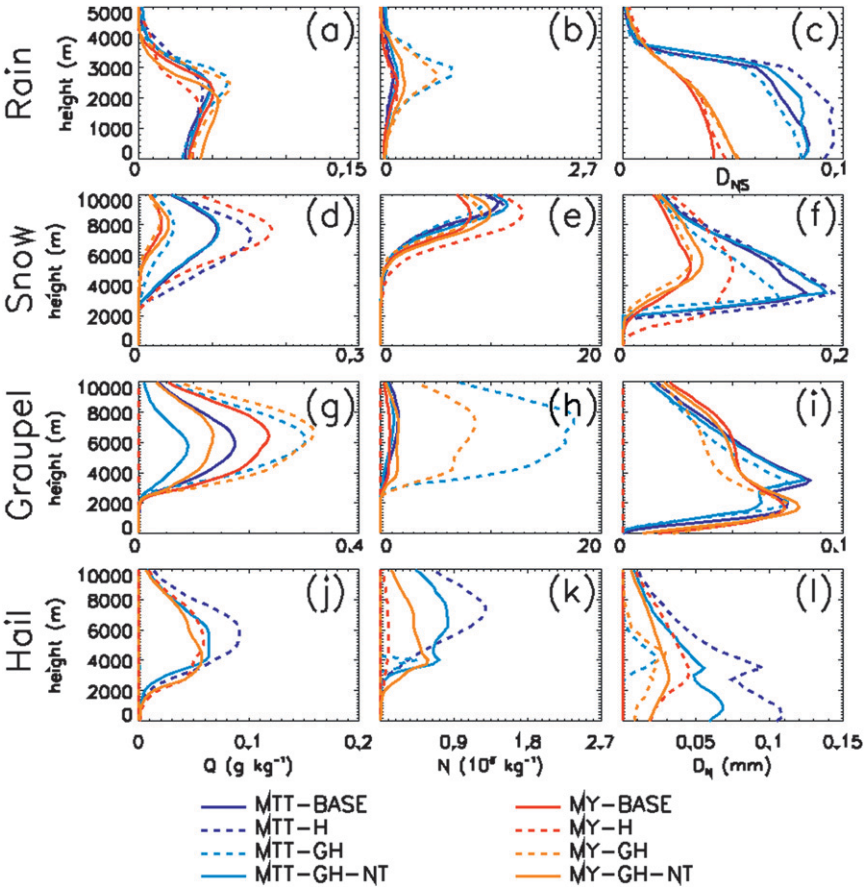

FIG. 10. As in Fig. 3, but for the experiments on the number of ice categories.

to decrease by 20% in the MTT-GH and the MY-GH experiments compared to baseline (Tables 4, 5).

Differences in the vertical profiles of graupel and hail between our graupel-only, hail-only, and graupel-plus-hail experiments resemble those found by MM11 for their experiments on the impact of graupel and hail on the simulation of an idealized 3D supercell. Vertical profiles of hail (Fig. 10j) reveal that, although both hail and graupel processes are parameterized, hardly any hail occurs in MTT-GH and MY-GH, which makes them resemble their counterparts that have only graupel. The main reason for this lack of hail is that both schemes implement a size threshold of 5 mm (for the mass-weighted mean diameter), below which hail is converted back to graupel at every time step. This effectively prevents hail from growing. To investigate the impact of this threshold, an additional experiment was conducted with both hail and graupel but without the threshold that converts hail back to graupel (MTT-GH-NT and MY-GH-NT). For surface precipitation, the removal of this threshold makes the experiments with both hail and graupel resemble more closely the hail-weighted experiments (MTT-H and MY-H). Graupel number concentration in the experiments without the graupel/hail threshold is not enhanced as dramatically as in the experiments with the threshold (Fig. 10h). Therefore, graupel deposition and sublimation, as well as the associated latent heat release, do not increase as much in the MTT-GH-NT experiment. Because graupel deposition and sublimation are not parameterized in the MY-GH experiment, the impact of removing the threshold is less obvious. Latent heat release increases somewhat in the MY-GH-NT experiment. This is probably associated with the more intense cold pools, as large hail reaches the surface. The probable reason for larger graupel number concentration in the experiments with the graupel–hail threshold (MTT-GH and MY-GH) is that a considerable number of hailstones are produced at every time step in these experiments, which are subsequently converted to graupel as long as the hail size remains small enough. Because graupel tends to fall much slower than hail, this eventually leads to a large accumulation of graupel particles aloft. From the vertical profiles (Figs. 10g,j), hail and graupel coexist in equally large quantities in the

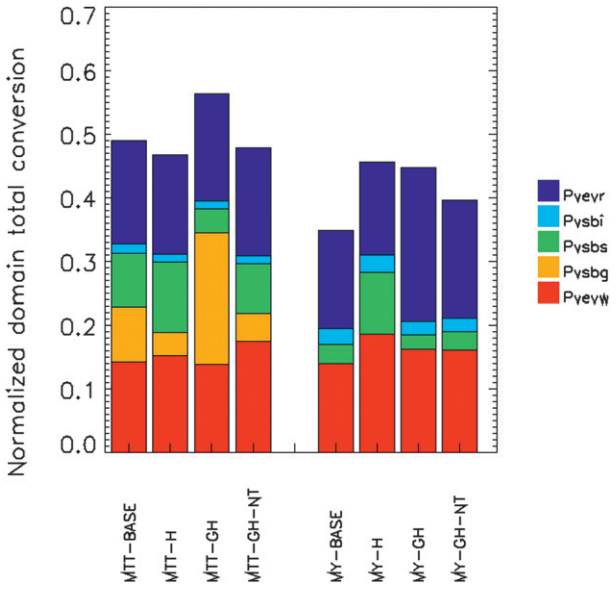

FIG. 11. As in Fig. 5, but for the experiments on the number of ice categories.

MTT-GH-NT and MY-GH-NT experiments. Because the behavior of these experiments is more like the hail-only experiments, domain-maximum precipitation is also enhanced (Tables 4, 5).

c. *Conversion process formulations*

As described in section 3a, the MTT and MY schemes exhibit very different behaviors in terms of surface-precipitation characteristics (Tables 4, 5). Typically, MY produces 20%–30% more surface precipitation, whereas the precipitation extremes are twice as large. Previous sections have shown that one of the key differences between the schemes is that MY tends to favor riming, whereas MTT tends to favor depositional growth (for this idealized case). Because the latent heat released by deposition is about an order of a magnitude larger than that associated with riming, this leads to more latent heat being released in MTT (Table 4). Figure 13 shows the vertical profile of the latent heating associated with depositional growth, riming, and condensation. Although latent heating associated with depositional growth (riming growth) accounts for 30% (7%) of the total latent heat released within the updrafts in the MTT scheme, this drops to about 7% (9%) in the MY scheme (almost all other latent heat release is due to condensation). This accounts for a 10%–20% larger latent heat release in the MTT scheme. On the other hand, Tables 4 and 5 also show that PE is typically 30%–60% larger in the MY scheme, mainly associated with less condensate being returned to vapor by sublimation processes outside the updraft cores. Recall that less snow is present in the MY scheme (and hence less snow sublimation occurs) and graupel deposition–sublimation is not parameterized in this scheme. The net effect of a much higher PE and a slightly lower latent heat in the MY scheme is an increase in surface precipitation. To understand further the origin of these differences, a series of experiments gradually replaced the conversion process formulations of the MTT scheme by those of the MY scheme.

The first experiment consisted of implementing the warm rain scheme of MY into MTT (MTT-WM). Details of the particular modifications that were made in this experiment are listed in appendix B (e.g., melting of graupel and snow were also modified in this experiment). The warm rain scheme only slightly increases the domain-average precipitation, but it is responsible for the large difference in domain-maximum precipitation between the MY and the MTT schemes (Table 4 and Fig. 14). Domain-maximum precipitation increases by nearly 80%, which is close to the value obtained in MY. One of the differences between the warm rain formulations of both schemes is the representation of collisional drop breakup. MM11 identified the collisional breakup of drops as one of the major differences between both schemes in terms of rain-size distributions and cold-pool development. Both schemes follow Verlinde and Cotton (1993) to calculate the combined effect of rain self-collection and collisional drop breakup,

$$\left.\frac{dN_R}{dt}\right|_{\text{self+brk}} = -\text{EC} \times \text{NRAGR}, \tag{6}$$

where NRAGR represents rain self-collection and EC is the collection efficiency defined as

$$\text{EC} = \begin{cases} 1, & D_{\text{NR}} < \text{Thr} \\ 2 - \exp[2300(D_{\text{NR}}) - \text{Thr}], & D_{\text{NR}} \geq \text{Thr} \end{cases}. \tag{7}$$

As soon as the number-weighted mean drop diameter D_{NR} grows larger than a threshold diameter Thr, EC becomes smaller than 1 and starts to counterbalance the number of raindrops lost by self-collection. Hence, collisional drop breakup is represented implicitly by increasing the number concentration of raindrops. Although MY applies a Thr of 600 μm, MTT applies a lower value of 300 μm, yielding a more intense breakup in MTT.

To understand the sole impact of drop breakup, an additional experiment was performed that was identical to the MTT-WM experiment, but leaving the collisional drop breakup as in the original MTT experiment (MTT-WM-BRK). From Table 4, this experiment has little impact on domain-average precipitation, consistent with MM11. However, this experiment brings the domain-maximum

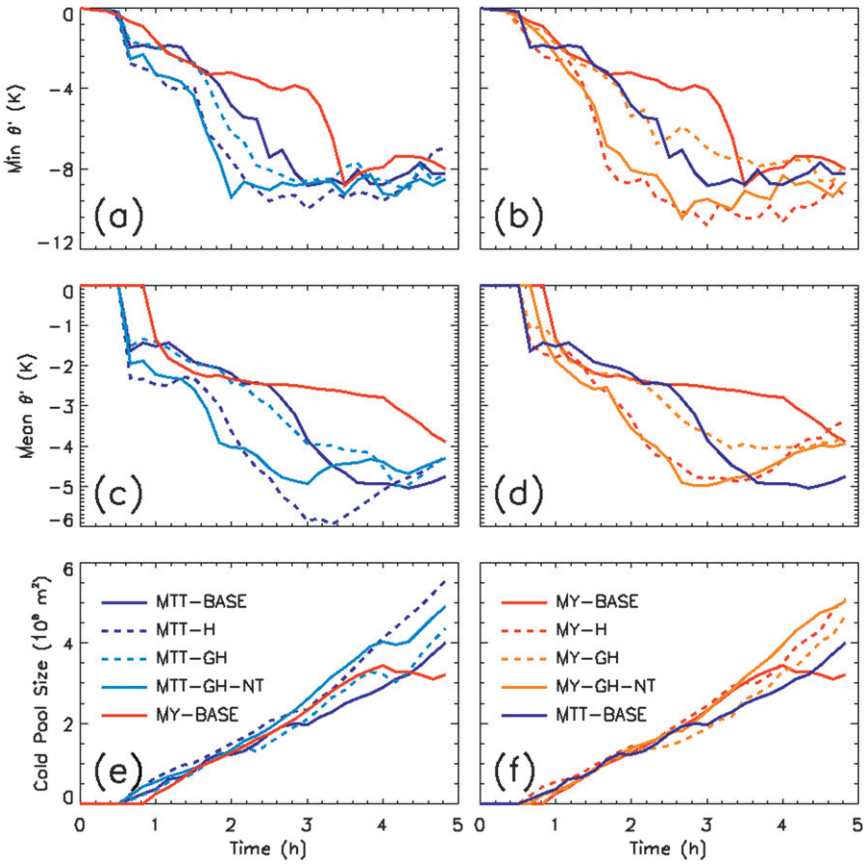

FIG. 12. As in Fig. 6, but for the experiments on the number of ice categories.

precipitation back to the value obtained in the MTT-BASE experiment, indicating that collisional drop breakup is the main factor determining the differences in peak precipitation between the schemes. Figure 15 shows the vertical profiles of rain mixing ratio, drop size, and evaporation that are associated with the location of maximum-domain-precipitation accumulation. Clearly, the lower threshold used for drop breakup in the MTT scheme limits largest drop sizes to be much smaller than those in MY, leading to slower fallout. Note that the vertical profile of rain mixing ratio in the MTT-WM-BRK experiment is not entirely the same as in the MTT-BASE experiment. Larger mixing ratios are present aloft in the MTT-WM-BRK experiment but, because rain evaporation is larger, the eventual fallout to the surface becomes similar for these two experiments (Figs. 15a,c). In the MTT-WM experiment, rain evaporation is similar to the MTT-WM-BRK experiment, despite much larger mixing ratios, because of the presence of larger raindrops. The increase of peak surface precipitation in the MTT-WM experiment seems to be compensated by a reduction in accumulated surface precipitation in the frontal area of the squall line (Fig. 14), yielding no significant impact on the domain-average precipitation (Table 4). This reduction is due to the more vigorous outflow in MTT-BASE continuously generating new cells near the outflow boundary and enhancing the squall-line propagation, as can be seen on the cross sections in Fig. 16. Indeed, the smaller drops associated with the different breakup formulation in MTT-BASE (and MTT-WM-BRK) favor more evaporative cooling and stronger rear-to-front outflow. Figure 17 shows that the MTT-WM experiment is also associated with a reduction in snow mixing ratios (Fig. 17d). This was found to be associated with differences in cloud drop activation between the schemes (not shown). The MTT scheme typically produces larger cloud drop number concentrations than the MY scheme, mainly below 8000-m altitude, which seems to favor snow riming growth at the expense of graupel riming growth.

The second step toward unraveling the differences between the MY and MTT schemes involved also replacing the formulations dealing with depositional growth and ice-to-snow autoconversion in MTT-WM with those of MY (MTT-WM-ICE). This experiment leads to a significant increase in domain-average surface precipitation of about 20%, whereas the domain maximum increases by

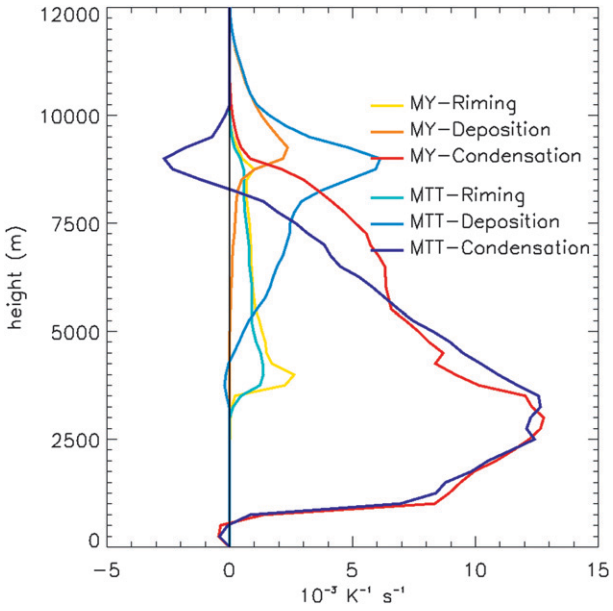

FIG. 13. Vertical profile of domain- and time-average latent heat released within updrafts (vertical velocity >1 m s^{-1}) associated with riming, deposition, and condensation for the MY-BASE (red) and the MTT-BASE (blue).

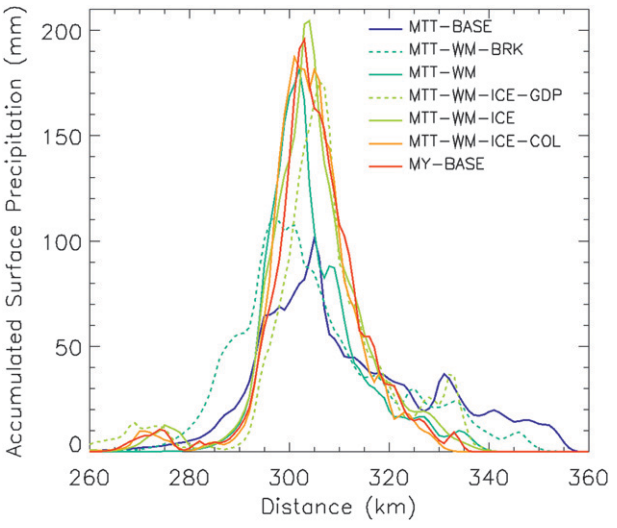

FIG. 14. As in Fig. 2, but for the experiments on the conversion term formulations.

10%. The surface-precipitation enhancement is associated with a 20% increase in PE. The main reason for this increase is the absence of graupel deposition–sublimation in the MY scheme (and hence in the MTT-WM-ICE experiment). This is also demonstrated by an additional experiment equal to MTT-WM-ICE, but with graupel sublimation–deposition included (MTT-WM-ICE-GDP). This experiment has a similar PE as MTT-WM and has a reduced surface precipitation compared to MTT-WM-ICE (Table 4). This is also clear from Fig. 18, which shows the normalized total amount of water vapor returned by microphysical processes for all of the conversion term formulation experiments. Graupel sublimation returns significant amounts of condensate back to the vapor phase in the MTT-BASE experiment, which lowers the PE. Not implementing the sublimation of graupel leads to higher PE and also larger precipitation fallout. It can be seen that the spatial distribution of accumulated precipitation in Fig. 14 is broadened in the MTT-WM-ICE experiment. Furthermore, PE in the MTT-WM-ICE experiment increases further because of less snow depositional growth (Fig. 18), which is associated with the less-active snow deposition formulation used in MY as compared to the formulations of Harrington et al. (1995) used in MTT. Figure 19 shows the impact of each of the conversion term formulation experiments on the sinks and sources of the snow mixing ratio. The reduction in snow depositional growth is partly compensated by more ice-to-snow autoconversion in the MTT-WM-ICE experiment, which leads to a rather minor change in the snow mixing ratios.

The last step in systematically converting the MTT scheme into the MY scheme consisted of implementing the collection growth formulations of MY in the MTT-WM-ICE experiment (MTT-WM-ICE-COL). This slightly reduces the domain-average and maximum precipitation, bringing those values in close agreement with the MY scheme (Tables 4, 5). Graupel growth in this experiment is favored further at the expense of snow growth, which reduces the snow mixing ratios to the amounts in the MY experiment (Fig. 17d). This is also clear from Fig. 19, which indicates that the only significant growth terms for snow that remain are the autoconversion from cloud ice and the depositional growth. Graupel mixing ratio does not increase because of a larger downward flux associated with the smaller number concentration of larger particles. The reduction in snow amount further reduces the amount of condensate that can sublimate back to the vapor phase and hence further enhances PE. However, latent heat release is decreased as well, leading to a small reduction in domain-average surface precipitation. The reason for the differences in snow mixing ratios between the MY and MTT schemes hence seems to be a combination of factors, including differences in cloud drop activation, snow depositional growth, and collection efficiencies.

4. Discussion and conclusions

A challenge to learning from comparisons of deep convection simulations with observations is a lack of understanding for the reasons of variability among

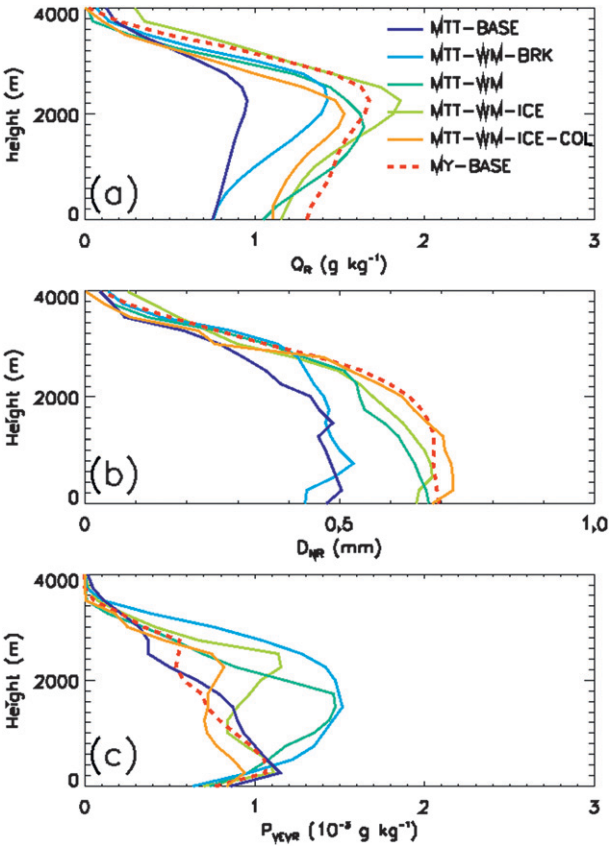

FIG. 15. As in Fig. 4, but for the experiments on the conversion term formulations.

different models. If it is unknown why equally complex models can exhibit substantially different behavior in terms of surface precipitation, it is hard to provide sound recommendations to model developers as to which aspects of the models require improvement. It is also often only vaguely understood how additional complexity in models affects the details of their behavior. To address these issues, this work examined the role of systematically adding complexity to microphysics schemes in idealized squall-line simulations within the framework of two commonly used two-moment bulk microphysics schemes.

We have shown that the explicit prediction of the number concentration for all precipitating hydrometeors is crucial because many important physical features, such as size sorting, are difficult to represent without it. Size sorting allows the mean particle diameter to be larger during sedimentation to the surface, which makes the particles less prone to evaporation and thus enhances surface precipitation. This was found to impact precipitation extremes. In contrast to many previous studies, we found that the explicit treatment of graupel number concentration was important to reducing cold-pool development. Size sorting allowed the largest graupel particles to accumulate around the freezing level and subsequently melt into larger raindrops that were less prone to evaporation. Thus, cold-pool intensity was significantly reduced mainly when two-moment rain was combined with a two-moment graupel treatment. A 10%–15% decrease in surface precipitation and a narrowing of the spatial surface-precipitation distribution in the two-moment graupel experiments are associated with the weaker cold outflow, which slows the squall-line propagation. It was further shown that hybrid schemes, combining a two-moment representation for certain species with a one-moment representation for other species, might lead to excessive number concentrations for the two-moment species and might not be physically consistent.

Second, similar to many previous studies (e.g., Gilmore et al. 2004; Van Weverberg et al. 2011b; MM11), we found colder cold pools in simulations containing hail only as compared to simulations containing graupel only. On the other hand, the sensitivity of surface precipitation to the representation of the rimed ice species (graupel or hail) was found to be smaller compared to those studies. It is uncertain at this time whether the reason for the difference is because most of the previous research dealt with idealized simulations of supercells or whether it is because those simulations were rather short. Bryan and Morrison (2012) also found a somewhat larger sensitivity of precipitation (up to 30% more precipitation when the rimed species was hail) for their 9-h simulations of idealized 3D squall lines as compared to our simulations (15% more precipitation when the rimed species was hail). Van Weverberg et al. (2011c, manuscript submitted to *Quart. J. Roy. Meteor. Soc.*) suggested that sensitivity to the nature of the largest rimed ice species becomes more pronounced as updrafts become stronger; the initial vertical profile used by Bryan and Morrison (2012) indeed had twice as much convective available potential energy and hence stronger updrafts compared to our simulations. Our simulations where both hail and graupel were included showed that adding ice categories does not have a very large impact on domain-average surface-precipitation behavior. Similar to MM11, we found that simulations with formulations for both hail and graupel hardly initiated any hail. However, we showed that these simulations are very sensitive to the threshold that determines the minimum size for hail to be sustained. The hail that is produced by these simulations typically is too small to be sustained and hence is converted back to graupel. Although the basis of this threshold is that hail embryos are typically larger than 5 mm, the scheme seems to be

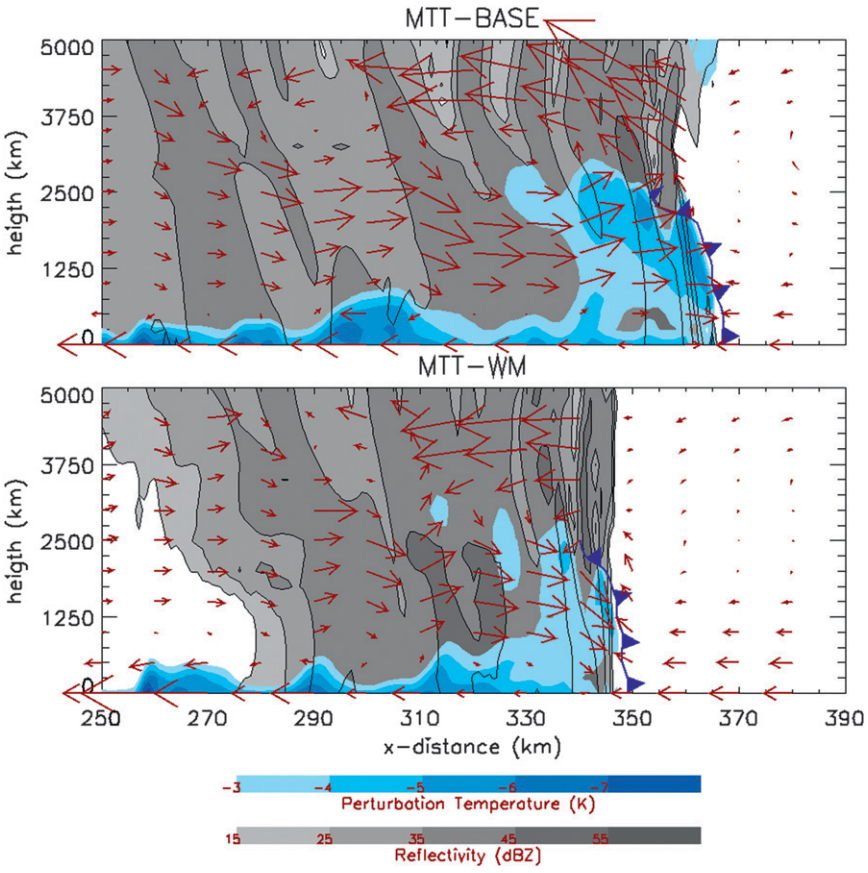

FIG. 16. Vertical cross sections through the squall line 5 h into the simulation for the (top) MTT-BASE and (bottom) MTT-WM experiments. Gray shading is radar reflectivity, and blue shading is cold-pool intensity (perturbation potential temperature). Arrows indicate the flow within the squall line, and the frontal outflow boundary (gust front) is denoted with blue triangles.

too stringent on hail initiation. Further, the way the threshold is implemented allows duplication of several production terms for graupel, leading to large graupel mixing ratios and number concentrations. Simulations behavior swings between the graupel-only experiments and the hail-only experiments depending on the application of the threshold. This finding indicates a need for a more physical treatment of the graupel-to-hail conversion: for instance, based on the amount of wet growth rather than on the size of the graupel particle.

Last, we have shown that, using identical size distribution assumptions and number of ice categories, very different behaviors still exist between the MTT and MY schemes in terms of surface precipitation and moist processes aloft, comparable to what MM11 found. We demonstrated that, although the MTT scheme behaves as a deposition-dominated scheme (more snow) with low precipitation efficiency, MY is dominated by riming process (more graupel) with high precipitation efficiency. MTT typically produces up to 30% less domain-average precipitation and only 50% of the peak precipitation that MY produces. The lower precipitation efficiency in the MTT scheme is associated mainly with graupel deposition–sublimation, which is not parameterized in the MY scheme. A recommendation for model development would be to include the sublimation of graupel in microphysics schemes, because it might return significant amounts of condensate to the vapor phase outside of the convective cores, reducing the precipitation efficiency. The absence of graupel sublimation in the MY scheme—and hence the higher precipitation efficiency—was the main factor responsible for the differences in domain-average surface precipitation between the MTT and the MY schemes. Domain-maximum precipitation differences, however, were almost entirely due to the different treatments of collisional drop breakup between the schemes. Breakup in the MTT scheme occurs at drop sizes only half as those in the MY scheme. Because of the smaller drops in the region of heavy precipitation in the MTT scheme, domain-maximum accumulated

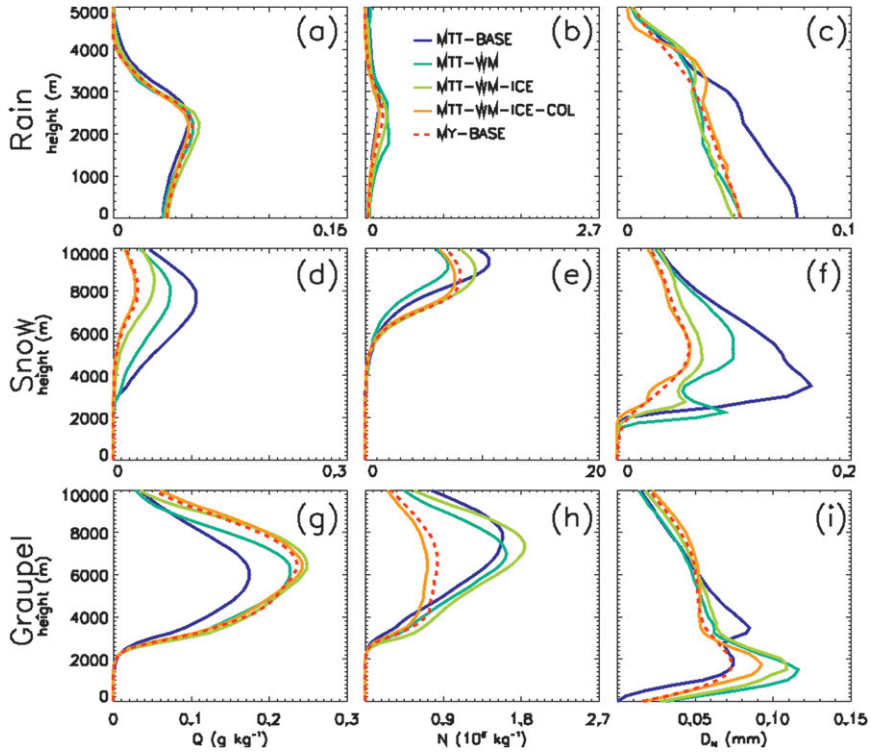

FIG. 17. As in Fig. 3, but for the experiment on the conversion term formulations.

precipitation was much smaller compared to the MY scheme. Differences in terms of snow amount aloft between the schemes were associated with an amalgam of processes, including cloud activation, snow depositional growth, and collection efficiencies.

It should be stressed that our findings are based on 2D simulations for a squall-line environment. Some of the differences between the MTT and MY schemes, as well as the sensitivities of both schemes to the number of ice categories or the number of predicted moments, might be

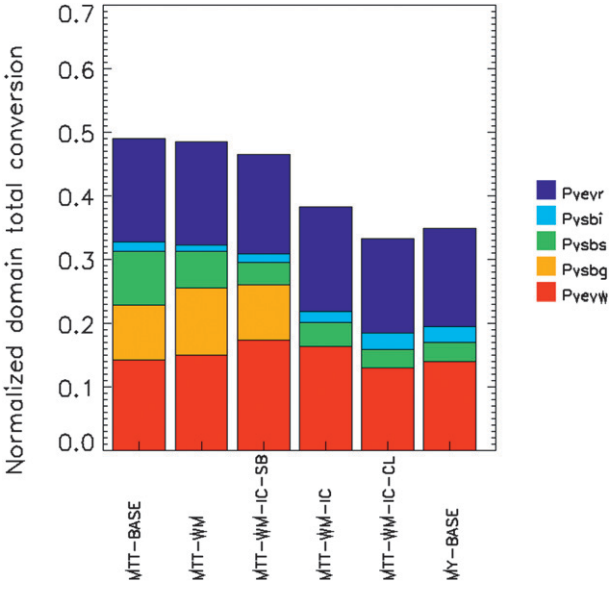

FIG. 18. As in Fig. 5, but for the experiments on the conversion term formulations.

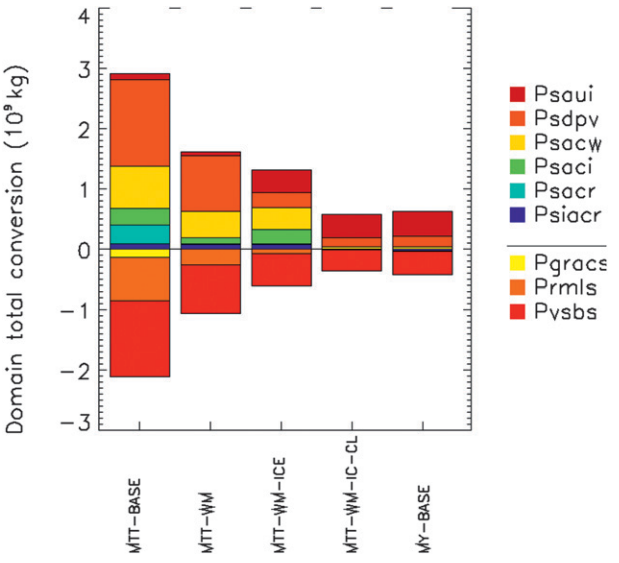

FIG. 19. Domain- and time-integrated total sinks and sources for the snow category associated with microphysical processes (given in legend) for all experiments on the conversion term formulations.

dependent on the environmental sounding and on the model setup. It would therefore be worthwhile to repeat these experiments for different environments or using a 3D approach. Indeed, previous research suggested that 3D simulations may experience more entrainment (Petch et al. 2008) and stronger updrafts (Phillips and Donner 2006). Nevertheless, this study adds to the general understanding of the role of microphysics in convection-resolving simulations, and the physical mechanisms proposed for the sensitivities probably apply under different environmental conditions as well. Key findings of this study will be examined further and evaluated against recent observations in the central United States in a 3D framework.

This research has pointed to the importance of raindrop sizes and evaporation rates on surface precipitation. Therefore, a strong need exists for observational data on vertical profiles of rain mixing ratio and drop sizes in order to determine better approaches for microphysics modeling. Over the past years, the focus in microphysics modeling often has been on the role of size distribution assumptions on moist processes and surface precipitation (e.g., bulk versus spectral approaches, graupel versus hail, two moment versus one moment), but an equally large variability is introduced by differences in the microphysical conversion term formulations. Thus, we recommend that improved formulations of collection, deposition, and melting, based on laboratory experiments and field campaigns, should be one of the primary foci for model improvement over the next years.

Acknowledgments. We thank Wuyin Lin and Yangang Liu for stimulating discussions. The research by K. Van Weverberg and A. M. Vogelmann was supported by the U.S. Department of Energy's Atmospheric Science Program Atmospheric System Research, an Office of Science Office of Biological and Environmental Research program, under Contract DE-AC02-98CH10886, and by the Earth System Modeling Program via the FASTER project (http://www.bnl.gov/esm). Hugh Morrison was partially supported by U.S. DOE ARM DE-FG02-08ER64574, NOAA Grant NA08OAR4310543, and the NSF Science and Technology Center for Multiscale Modeling of Atmospheric Processes (CMMAP) managed by Colorado State University under Cooperative Agreement ATM-0425247. We also thank Amy Solomon for providing the code on cloud activation in the MTT scheme.

APPENDIX A

Conversion Term Overview and Acronyms

TABLE A1. Overview of microphysical conversion terms. All acronyms are constructed so that the second (last) letter is the category experiencing the gain (loss). The third and fourth letter indicate the process associated with the conversion: ev (evaporation), cd (condensation), sb (sublimation), dp (deposition), ac (accretion), nt (initiation), au (autoconversion), sp (splintering), and fr (freezing). When three categories are involved, the third letter indicates the category not experiencing any loss or gain. An X in the table denotes that the process is active in the respective baseline microphysics scheme (MTT-BASE or MY-BASE).

Acronym	MTT	MY	Explanation
Pwcdv	X	X	Cloud water condensation
Pvevw	X	X	Cloud water evaporation
Pintv	X	X	Initiation of cloud ice at the expense of water vapor
Pidpv	X	X	Cloud ice depositional growth at the expense of water vapor
Pvsbi	X	X	Cloud ice sublimation
Pvevr	X	X	Rain evaporation
Psdpv	X	X	Snow depositional growth
Pvsbs	X	X	Snow sublimation
Pgdpv	X		Graupel depositional growth
Pvsbg	X		Graupel sublimation
Pifrw	X	X	Homogeneous freezing of cloud water to cloud ice
Pisspw	X		Rime-splintering of cloud water accreted by snow (generation of ice)
Pigspw	X		Rime-splintering of cloud water accreted by graupel (generation of ice)
Piacw	X		Collection of cloud water by cloud ice
Prauw	X	X	Autoconversion of cloud water to rain
Pracw	X	X	Collection of cloud water by rain
Psacw	X	X	Collection of cloud water by snow
Pgacw	X	X	Collection of cloud water by graupel
Pgsacw	X		Collection of cloud water by snow adding to graupel
Pisspr	X		Rime-splintering of rain accreted by snow (generation of ice)

TABLE A1. (*Continued*)

Acronym	MTT	MY	Explanation
Pigspr	X		Rime-splintering of rain accreted by graupel (generation of ice)
Pisps		X	Rime-splintering of snow (generation of ice)
Pispg		X	Rime-splintering of graupel (generation of ice)
Pgraci	X	X	Collection of cloud ice by rain adding to graupel
Psraci	X	X	Collection of cloud ice by rain adding to snow
Psaui	X	X	Autoconversion of cloud ice to snow
Psaci	X	X	Collection of cloud ice by snow
Pgaci		X	Collection of cloud ice by graupel
Prmli	X	X	Melting of cloud ice to rain
Prmls	X	X	Melting of snow to rain
Prmlg	X	X	Melting of graupel to rain
Pgiacr	X	X	Collection of rain by cloud ice adding to graupel
Psiacr	X	X	Collection of rain by cloud ice adding to snow
Psacr	X	X	Collection of rain by snow
Pgsacr	X	X	Collection of rain by snow adding to graupel
Pgacr	X	X	Collection of rain by graupel
Pgfrr	X		Homogeneous freezing of rain to graupel
Pgaus		X	Autoconversion of snow to graupel

APPENDIX B

Conversion Term Experiments

The following conversion term formulations in MTT were modified to match those in MY in each of the respective experiments (abbreviated conversion term formulations are explained in appendix A):

MTT-WM: All conversion terms associated with warm rain processes as well as all melting processes (Pvevr, Pwcdv, Pvevw, Pracw, Prauw, Psmlt, Pimlt, Pgmlt, breakup, and cloud activation).
MTT-WM-BRK: As in MTT-WM, but with breakup formulated as in the MTT scheme (breakup threshold of 300 μm).
MTT-WM-ICE: As in MTT-WM, but also all processes associated with deposition and solid autoconversion (Pgdpv, Pvsbg, Psdpv, Pvsbs, Pidpv, Pvsbi, Psaui, Pintv, Pifrw, and Pgaus).
MTT-WM-ICE-COL: As in MTT-WM-ICE, but also all collection terms.

APPENDIX C

Additional Experiments to the Number of Moments

It was shown in section 3a that it was not until graupel became two moment that cold pools weakened and the spatial distribution of precipitation narrowed and became more peaked. To understand the role of graupel in more detail, three additional experiments were conducted, combining two-moment graupel with several combinations of one- and two-moment snow and rain (1R1S2G, 1R2S2G, and 2R1S2G).

From Fig. C1, it is clear that the precipitation distribution only narrows and becomes more peaked when two-moment graupel is combined with two-moment rain (BASE and 2R1S2G). If one-moment rain is combined with two-moment graupel (1R1S2G and 1R2S2G), the impact of graupel size sorting on rain-size distribution becomes very small, as rain number concentration is only diagnosed from the rain mixing ratio. Figure C2 shows the cold-pool evolution for the different combinations of one- and two-moment rain and snow with two-moment graupel. Again, it is clear that a two-moment representation of rain is required for two-moment graupel to impact the cold-pool intensity. However, cold pools are not weakened as much in the 2R1S2G experiments compared to the BASE experiments. The reason for this behavior can be found in Fig. C3, showing the vertical profile of graupel mixing ratio and number concentration in the different experiments. A gain in graupel number concentration mainly originates from losses in rain and snow number concentrations in both the MY and the MTT schemes. If snow (or rain) is not two moment, while graupel is two-moment, this implies that imbalances might occur. Indeed, a gain in graupel number concentration will not necessarily be accompanied with an equal loss in snow (or rain) number concentration, because the number concentration of the latter is always diagnosed from the snow (or rain) mixing ratio. Therefore, snow (and rain) will be nearly inexhaustible sources of graupel number. From Fig. C3, this might lead to very large

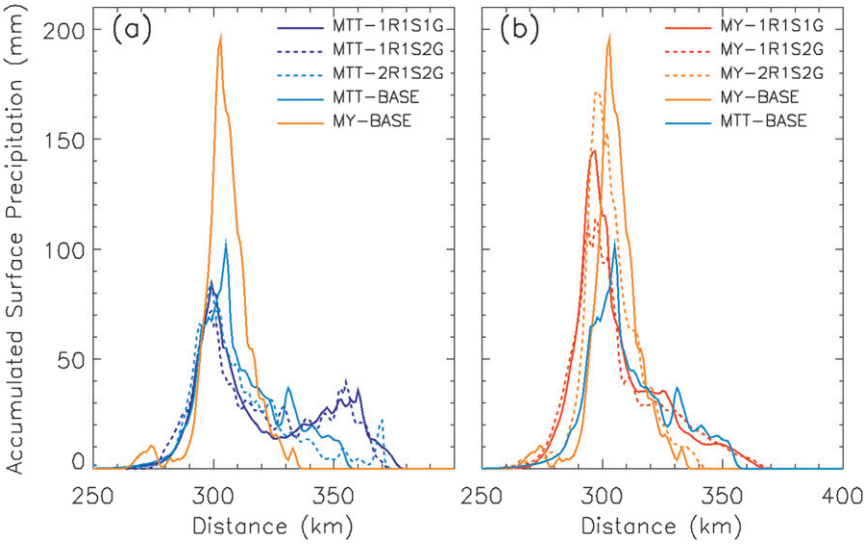

FIG. C1. Spatial distribution of accumulated surface precipitation over the full time integration of 5 h for the additional experiments on the number of predicted moments for (a) the MTT scheme (in blue) and (b) the MY scheme (in red). The baseline simulations of the MY and MTT schemes have been added for reference.

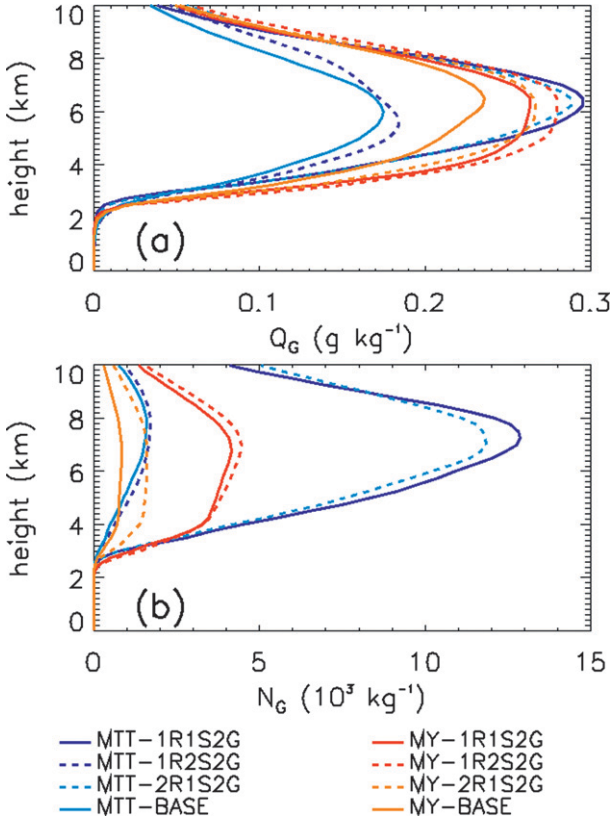

FIG. C2. Time evolution of mean cold-pool intensity for the additional experiments on the number of predicted moments for (a) the MTT scheme and (b) the MY scheme. Cold pools are defined by the −1-K isotherm of surface potential temperature perturbation. The baseline simulations of the MY and MTT schemes have been added for reference.

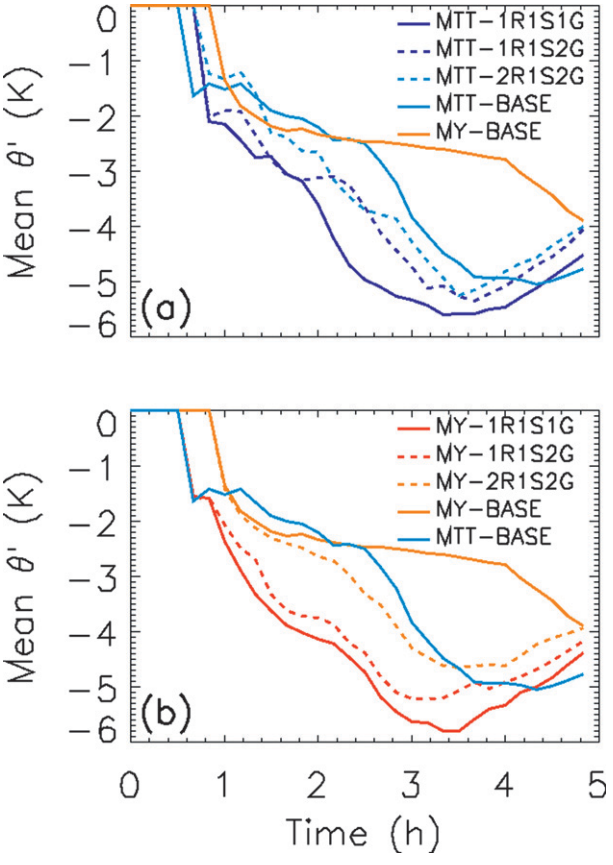

FIG. C3. Domain- and time-averaged vertical profiles of (a) graupel mixing ratio and (b) graupel number concentration for the additional experiments on the number of predicted moments. MTT experiments are represented in blue and MY experiments are in red.

mixing ratios of graupel, much larger than in the fully two-moment schemes. In the 2R1S2G experiment, for instance, graupel number is larger than in the BASE experiments for this reason, and hence the more numerous (and hence smaller) graupel particles also melt in to more numerous (and hence smaller) raindrops. These smaller raindrops are more prone to evaporation and hence cold pools are not weakened as much as compared to the fully two-moment (BASE) experiments. This implies that a two-moment approach for all precipitation species is required to realistically simulate the surface precipitation and cold-pool evolution.

REFERENCES

Bryan, G. H., and H. Morrison, 2012: Sensitivity of a simulated squall line to horizontal resolution and parameterization of microphysics. *Mon. Wea. Rev.,* **140,** 202–225.

Cohard, J. M., and J. P. Pinty, 2000: A comprehensive two-moment warm microphysical bulk scheme. I: Description and tests. *Quart. J. Roy. Meteor. Soc.,* **126,** 1815–1842.

Cohen, C., and E. W. McCaul Jr., 2006: The sensitivity of simulated convective storms to variations in prescribed single-moment microphysics parameters that describe particle distribution sizes and numbers. *Mon. Wea. Rev.,* **134,** 2547–2565.

Cooper, W. A., 1986: Ice initiation in natural clouds. *Precipitation Enhancement—A Scientific Challenge, Meteor. Monogr.,* No. 43, Amer. Meteor. Soc., 29–32.

Cotton, W. R., M. A. Stephens, T. Nehrkorn, and G. J. Tripoli, 1982: Colorado State University three-dimensional cloud/mesoscale model. Part 2: Ice phase parameterization. *J. Rech. Atmos.,* **16,** 295–320.

Dawson, D. T., M. Xue, J. A. Milbrandt, and M. K. Yau, 2010: Comparison of evaporation and cold pool development between single-moment and multimoment bulk microphysics schemes in idealized simulations of tornadic thunderstorms. *Mon. Wea. Rev.,* **138,** 1152–1171.

Dudhia, J., 1989: Numerical study of convection observed during the winter monsoon experiment using a mesoscale two-dimensional model. *J. Atmos. Sci.,* **46,** 3077–3107.

Ferrier, B. S., 1994: A double-moment multiple-phase four-class bulk ice scheme. Part I: Description. *J. Atmos. Sci.,* **51,** 249–280.

——, W.-K. Tao, and J. Simpson, 1995: A double-moment multiple-phase four-class bulk ice scheme. Part II: Simulations of convective storms in different large-scale environments and comparisons with other bulk parameterizations. *J. Atmos. Sci.,* **52,** 1001–1033.

Fovell, R. G., G. L. Mullendore, and S.-H. Kim, 2006: Discrete propagation in numerically simulated nocturnal squall lines. *Mon. Wea. Rev.,* **134,** 3735–3752.

Gilmore, M. S., J. M. Straka, and E. N. Rasmussen, 2004: Precipitation uncertainty due to variations in precipitation particle parameters within a simple microphysics scheme. *Mon. Wea. Rev.,* **132,** 2610–2627.

Harrington, J. Y., M. P. Meyers, R. L. Walko, and W. R. Cotton, 1995: Parameterization of ice crystal conversion processes due to vapor deposition for mesoscale models using double-moment basis functions. Part I: Basic formulation and parcel model results. *J. Atmos. Sci.,* **52,** 4344–4366.

Kessler, E., 1969: *On the Distribution and Continuity of Water Substance in Atmospheric Circulations*. *Meteor. Monogr.,* No. 32, Amer. Meteor. Soc., 84 pp.

Khain, A., A. Pokrovsky, and I. Sednev, 1999: Some effects of cloud-aerosol interaction on cloud microphysics structure and precipitation formation: Numerical experiments with a spectral microphysics cloud ensemble model. *Atmos. Res.,* **52,** 195–220.

Kogan, Y. L., 1991: The simulation of a convective cloud in a 3D model with explicit microphysics. Part I: Model description and sensitivity experiments. *J. Atmos. Sci.,* **48,** 1160–1189.

Lin, Y.-L., R. D. Farley, and H. D. Orville, 1983: Bulk parameterization of the snow field in a cloud model. *J. Climate Appl. Meteor.,* **22,** 1065–1092.

Locatelli, J. D., and P. V. Hobbs, 1974: Fall speeds and masses of solid precipitation particles. *J. Geophys. Res.,* **79,** 2185–2197.

McCumber, M., W.-T. Tao, J. Simpson, R. Penc, and S.-T. Soong, 1991: Comparison of ice-phase microphysical parameterization schemes using numerical simulations of tropical convection. *J. Appl. Meteor.,* **30,** 985–1004.

Milbrandt, J. A., and M. K. Yau, 2005a: A multimoment bulk microphysics parameterization. Part I: Analysis of the role of the spectral shape parameter. *J. Atmos. Sci.,* **62,** 3051–3064.

——, and ——, 2005b: A multimoment bulk microphysics parameterization. Part II: A proposed three-moment closure and scheme description. *J. Atmos. Sci.,* **62,** 3065–3081.

——, and ——, 2006: A multimoment bulk microphysics parameterization. Part IV: Sensitivity experiments. *J. Atmos. Sci.,* **63,** 3137–3159.

——, ——, J. Mailhot, S. Belair, and R. McTaggart-Cowan, 2010: Simulations of an orographic precipitation event during IMPROVE-2. Part II: Sensitivity to the number of moments in the bulk microphysics scheme. *Mon. Wea. Rev.,* **138,** 625–642.

Morrison, H., and A. Gettelman, 2008: A new two-moment bulk stratiform cloud microphysics scheme in the Community Atmosphere Model, version 3 (CAM3). Part I: Description and numerical tests. *J. Climate,* **21,** 3642–3659.

——, and J. Milbrandt, 2011: Comparison of two-moment bulk microphysics schemes in idealized supercell thunderstorm simulations. *Mon. Wea. Rev.,* **139,** 1103–1130.

——, G. Thompson, and V. Tatarskii, 2009: Impact of cloud microphysics on the development of trailing stratiform precipitation in a simulated squall line: Comparison of one- and two-moment schemes. *Mon. Wea. Rev.,* **137,** 991–1007.

Petch, J. C., P. N. Blossey, and C. S. Bretherton, 2008: Differences in the lower troposphere in two- and three-dimensional cloud-resolving model simulations of deep convection. *Quart. J. Roy. Meteor. Soc.,* **134,** 1914–1946.

Phillips, V. T. J., and L. J. Donner, 2006: Cloud microphysics, radiation and vertical velocities in two- and three-dimensional simulations of deep convection. *Quart. J. Roy. Meteor. Soc.,* **132,** 3011–3033.

Reinhardt, T., and A. Seifert, 2006: A three-category ice scheme for LMK. *COSMO Newsletter,* No. 6, Consortium for Small-Scale Modelling, Germany, 115–120.

Rotunno, R., J. B. Klemp, and M. L. Weisman, 1988: A theory for strong, long-lived squall lines. *J. Atmos. Sci.,* **45,** 463–485.

Rutledge, S. A., and P. V. Hobbs, 1984: The mesoscale and microscale structure and organization of clouds and precipitation in mid-latitude cyclones. Part XII: A diagnostic modeling study of precipitation development in narrow cold-frontal rainbands. *J. Atmos. Sci.,* **41,** 2949–2972.

Seifert, A., and K. D. Beheng, 2001: A double-moment parameterization for simulating autoconversion, accretion and self-collection. *Atmos. Res.,* **59–60,** 265–281.

Skamarock, W. C., J. B. Klemp, J. Dudhia, D. O. Gill, D. M. Barker, W. Wang, and J. G. Powers, 2007: A description of the advanced research WRF version 2. NCAR Tech. Note NCAR/TN-468+STR, 88 pp.

Song, X., and G. J. Zhang, 2011: Microphysics parameterization for convective clouds in a global climate model: Description and single-column model tests. *J. Geophys. Res.,* **116,** D02201, doi:10.1029/2010JD014833.

Straka, J. M., and E. R. Mansell, 2005: A bulk microphysics parameterization with multiple ice precipitation categories. *J. Appl. Meteor.,* **44,** 445–466.

Sui, C. H., X. Li, and M.-J. Yang, 2007: On the definition of precipitation efficiency. *J. Atmos. Sci.,* **64,** 4506–4513.

Thompson, G., R. M. Rasmussen, and K. Manning, 2004: Explicit forecasts of winter precipitation using an improved bulk microphysics scheme. Part I: Description and sensitivity analysis. *Mon. Wea. Rev.,* **132,** 519–542.

Tripoli, G. J., and W. R. Cotton, 1980: A numerical investigation of several factors contributing to the observed variable intensity of deep convection over South Florida. *J. Appl. Meteor.,* **19,** 1037–1063.

van den Heever, S. C., and W. R. Cotton, 2004: The impact of hail size on simulated supercell storms. *J. Atmos. Sci.,* **61,** 1596–1609.

Van Weverberg, K., N. P. M. van Lipzig, and L. Delobbe, 2011a: The evaluation of moist processes in km-scale NWP models using remote sensing and in-situ data: Impact of size distribution assumptions. *Atmos. Res.,* **99,** 15–38.

——, ——, and ——, 2011b: The impact of size distribution assumptions in a simple microphysics scheme on surface precipitation and storm dynamics during a low-topped supercell case. *Mon. Wea. Rev.,* **139,** 1131–1147.

Varble, A., and Coauthors, 2011: Evaluation of cloud-resolving model intercomparison simulations using TWP-ICE observations: Precipitation and cloud structure. *J. Geophys. Res.,* **116,** D12206, doi:10.1029/2010JD015180.

Verlinde, H., and W. R. Cotton, 1993: Fitting microphysical observations of nonsteady convective clouds to a numerical model: An application of the adjoint technique of data assimilation to a kinematic model. *Mon. Wea. Rev.,* **121,** 2776–2793.

Weisman, M. L., and J. B. Klemp, 1984: The structure and classification of numerically simulated convective storms in directionally varying wind shears. *Mon. Wea. Rev.,* **112,** 2479–2498.

——, and R. Rotunno, 2004: ''A theory for strong, long-lived squall lines'' revisited. *J. Atmos. Sci.,* **61,** 361–382.